Cover Sheet:

Trace Element Analyses of Plagioclase from Troctolite 76535 and Implications for Mg-suite Petrogenesis

Isaiah SPRING[1], Ananya MALLIK[1], Jason KIRK[1], Pranabendu MOITRA[1], Richard HERVIG[2], and Lars BORG[3]

[1]University of Arizona Geosciences, Tucson, Arizona; [2]Arizona State University School of Earth and Space Exploration, Tempe, Arizona; [3]Lawrence Livermore National Laboratory, Livermore, California

This is a non-peer reviewed preprint submitted to EarthArXiv. This manuscript is currently in review with the journal of Meteoritics and Planetary Science. Data and python files used in this manuscript are available upon request.

Trace Element Analyses of Plagioclase from Troctolite 76535 and Implications for Mg-suite Petrogenesis

Isaiah SPRING[1], Ananya MALLIK[1], Jason KIRK[1], Pranabendu MOITRA[1], Richard HERVIG[2], and Lars BORG[3]

[1]University of Arizona Geosciences, Tucson, Arizona; [2]Arizona State University School of Earth and Space Exploration, Tempe, Arizona; [3]Lawrence Livermore National Laboratory, Livermore, California

***Correspondence**: Isaiah Spring, Geosciences, University of Arizona, 1040 E 4th Street 85721, Tucson, Arizona, USA, Email: IsaiahSpring@arizona.edu.

ABSTRACT

Certain Mg-suite samples display enrichment in incompatible elements, likely resulting from the assimilation of the material that crystallized at the very late stages of magma ocean (ur-KREEP). This study uses trace element analyses of plagioclase separates from sample 76535 to estimate the Rare Earth Element (REE) concentration of the Mg-suite parental liquid and assess the extent of contribution from ur-KREEP. Thirty-three trace elements, including REEs, were measured in the separates and the measured REEs reflect magmatic conditions being free from subsolidus alteration. The Mg-suite parental liquid was estimated using these REE data as targets for a Python-based forward model which employs a RhyoliteMELTS-defined liquid line of descent. The estimated parental liquid shows REE enrichments of 200 times chondritic levels for Light REEs and 20 times for Heavy REEs. Mixing models between the REE compositions of a potential Mg-suite primary liquid and modeled ur-KREEP indicate that 30-50% assimilation of ur-KREEP is required to reproduce the observed REE concentrations in the Mg-suite parental liquid. We demonstrate an approach to determine the petrogenesis of a sample by characterizing a very limited quantity of grains, in an effort to maximize the scientific output from current and future returned samples such as Artemis.

INTRODUCTION

The Mg-suite is a series of lunar highlands samples composed predominantly of anorthositic lithologies, which are chemically distinct from other lunar highlands terranes (Warner et al., 1976). The Mg-suite is characterized by an alkali content of 0.05 wt% K_2O, highly magnesian olivine (Fo > 80, where Fo = Mg/[Mg + Fe]), and highly calcic plagioclase (An > 90, where An = Ca / [Ca + Na + K]) (Dymek et al., 1975; Gooley et al., 1974, Snyder et al., 1999). Mg-suite samples are enriched in incompatible trace elements (Haskin et al., 1974; Gooley et al., 1974; Dymek et al., 1975) which has been designated a KREEP signature because of enrichments in potassium, rare-earth elements (REEs), and phosphorus. Explanations for the source of this signature have suggested the assimilation of the residual liquid created by 99% crystallization of the lunar magma ocean called ur-KREEP (Warren 1986; Hess 1994; Papike et al., 1998; Shervais and McGee, 1998; Shearer and Papike, 2005; Longhi et al., 2010; Elardo et al., 2012).

Aside from the Mg-suite, Mg-rich cumulates have also been identified in lunar meteorites (Treiman et al., 2010; Yamaguchi et al., 2010; Roberts et al., 2019; Gross et al., 2020; Cao et al., 2021; Hulsey et al., 2024; He et al., 2024) and in the Chang'e 5 samples (He et al., 2024). These

additional Mg-rich samples may be cogenetic with the Mg-suite. However, some are KREEP-poor compared to the Mg-suite (Treiman et al., 2010; He et al., 2024). The absence of a KREEP signature in these Mg-rich cumulates may be linked to lunar crustal dichotomy. Remote sensing data restricts enrichments of radioactive elements associated with ur-KREEP to the nearside Procellarum KREEP Terrane (PKT) and the farside South Pole-Aitken Terrane (SPAT) (Lawrence et al., 2000; Metzer et al., 1973, 1977; Jolliff et al., 2000; Martinot et al., 2020), while likely exposures of Mg-rich cumulates have been identified across the lunar surface (Lucey and Cahill, 2009; Klima et al., 2011; Jolliff et al., 2000; Taylor, 2009; Prissel et al., 2014a; Shearer et al., 2015; Hulsey et al., 2024). Much of these identified Mg-rich exposures lay outside the PKT, and SPAT, and may therefore be the source of the KREEP-poor Mg-rich cumulate samples. Additional petrogenetic differences may also exist between KREEP-rich and KREEP-poor Mg-rich samples, as suggested by James and Flohr (1983), Treiman and Gross (2015), Prissel et al. (2016), and Gross et al. (2020). The complex characteristics of Mg-suite samples have led to varying models for their formation. Shearer et al. (2015) provided a comprehensive summary of models for Mg-suite petrogenesis which include: (1) impact melting and differentiation (Taylor et al., 1993; Hess 1994; McKay et al., 1979), (2) co-magmatism with the primary FAN (Ferroan Anorthosite) crust (Wood, 1975; Longhi and Boudreau, 1979; McCallum, 1983) (3) post Lunar Magma Ocean (LMO) KREEP remelting and remobilization (Hess et al., 1978; Hess, 1989; Snyder et al., 1995) (4) decompression or radioactive decay induced melting of early LMO cumulates (Warren and Wasson, 1977; James and Flohr, 1983; Warren, 1986; Papike et al., 1994; Papike et al., 1996; Snyder et al., 1992), and (5) melting of a hybridized LMO cumulate and KREEP lithology in either the upper or lower mantle (Shearer et al., 2006; Shearer and Floss, 2000; Shearer and Papike, 1999, 2005; Elardo et al., 2012).

Shearer et al. (2015) present several lines of evidence opposing the impact melting model, including the required mass balance between the impactor and the crust, the depth of Mg-suite formation (30-50 km) in comparison to common buried impact melt sheet depths, and the pre-Nectarian ages of Mg-suite samples which are older than most large near-side craters. Consequently, models that incorporate decompression melting of rising cumulates as the source of the primary Mg-suite parental liquid, which subsequently interacts with ur-KREEP, forming the Mg-suite parental liquid, have gained favor in the lunar science community. This model can effectively reproduce the mineralogy of the Mg-suite and their trace element enrichments in Apollo Mg-suite samples (Elkins-Tanton et al., 2002; Laneuville et al., 2013). However, the necessity of an ur-KREEP contribution to Mg-suite petrogenesis has been questioned (e.g., Shearer et al., 2015; Elardo et al., 2020), and the nature of the temporal relationship between the Mg-suite, ur-KREEP, and FAN needs to be resolved.

To complete the objectives of this work and confirm a model for Mg-suite petrogenesis, it is essential to first reconcile its chronological relationship with FAN and ur-KREEP. While extrapolations from multiple geochronometers (Pb-Pb, Ar-Ar, Rb-Sr, and Sm-Nd) suggest that the Mg-suite is contemporaneous with FAN at 4359 ± 9 Ma (Borg et al., 2020) and ur-KREEP at 4368 ± 29 Ma (Gaffney and Borg, 2014; Snape et al., 2016; and Maurice et al., 2020), Nelson et al. (2021) demonstrated through diffusion chronology that Mg-suite plutonic bodies initially cooled more rapidly, placing their formation around 4.33 Ga. Ages consistent with this younger age are common in Mg-suite samples, having been observed in samples 78236 (4333 ± 59 Ma; Edmunson et al., 2009), 67667 (4349 ± 31 Ma and 4368 ± 67 Ma; Borg et al., 2020), and 77215 (4368±42 Ma; Zhang et al., 2021). This chronological data, clustered around 4.33-4.35 Ga,

suggests that the Mg-suite represents a pulse of magmatism occurring approximately 20 Ma after the segregation of FAN.

To elucidate the mechanisms behind the KREEP signature in the Mg-suite, further analyses of Mg-suite samples are required. The results of these analyses can then be used to model trace element concentrations in their parental liquids. Such an exercise might focus on REEs, given their sensitivity to magmatic processes and well-constrained partitioning behavior in lunar magmas. REEs also function as quantitative tracers of crystallization and fractionation processes (Hess, 1989) which are used to explore the petrogenesis of the parental liquid.

The first objective of this work is to re-analyze the trace elements in plagioclase from Mg-suite sample 76535-11 using microanalytical techniques. Sample 76535 was selected for this work as it is considered the most pristine Mg-suite sample (Warren, 1993). Previous studies (Haskin et al., 1974; Borg et al., 2017) have reported trace element concentrations for 76535 through solution-based analyses of mineral separates. Haskin et al. (1974) measured REEs in grain separates from 76535-21 and 76535-22 through isotope dilution. Borg et al. (2017) analyzed REE grain separates of 76535-11 using inductively coupled plasma mass spectrometry (ICP-MS).

Analyses of bulk mineral material limit observations of inter- and intra-grain heterogeneity. Plagioclase from 76535 (Nelson et al., 2021) and other Mg-suite samples (Shervais and McGee, 1998) contain notable albitic rims, which may be REE-rich, skewing the analysis. To address these issues, we utilized three microanalytical techniques to measure inter- and intra-grain chemistries: electron probe microanalysis (EPMA), secondary ion mass spectrometry (SIMS), and laser ablation inductively coupled plasma mass spectrometry (LA-ICP-MS). Thirty-three trace and minor elements were measured in this study, including but not limited to major elements, first-row transition elements (FRTE), rare-earth elements (REE), large-ion lithophile elements (LILE), and high field strength elements (HFSE). Seventeen of these elements have not been previously reported for plagioclase from 76535, and eleven have never been reported for any phase of 76535.

The second objective of this study is to build on these methods and estimate the true Mg-suite parental liquid by (1) utilizing the improved characterization of the REE concentrations within sample 76535 obtained for this work and using improved partitioning behaviors calibrated for lunar magmas, (2) verifying that the measured REE concentrations reflect magmatic conditions, and (3) employing a parental liquid forward model which more accurately estimates the Mg-suite parental liquid. The Earlier estimates of the REEs in the Mg-suite parental liquid performed by Haskin et al. (1974), Papike (1996), and Shervais and McGee (1998) are shown in figure 1. These estimates used experimentally determined partition coefficients to invert REE data from major phases within 76535 and other Mg-suite norites and troctolites. We note that this inversion method estimates the REE concentration of the liquid in equilibrium with the measured phases and is highly sensitive to variations in REE concentration and partition coefficient. The accuracy of the inversion also relies on the assumption that the measured REE concentrations reflect magmatic conditions and are free from subsolidus alteration. Given the lengthy subsolidus cooling history of 76535 (estimated cooling rate of 3.9 C/ Myr, Borg et al., 2017), there is a possibility of readjustment of REE abundances due to subsolidus diffusion, which needed to be accounted for. Furthermore, the estimated equilibrium liquids are likely more REE-enriched than the true Mg-suite parental liquid, as the phases measured in those studies were likely not on the

liquidus of the true parental liquid but were likely in equilibrium with a residual liquid along the liquid line of descent which is comparatively more REE-enriched (Treiman, 1996).

The final objective of this work is to constrain the extent of ur-KREEP assimilation to the Mg-suite parental liquid. Using the estimated parental liquid REE concentrations, we can explore

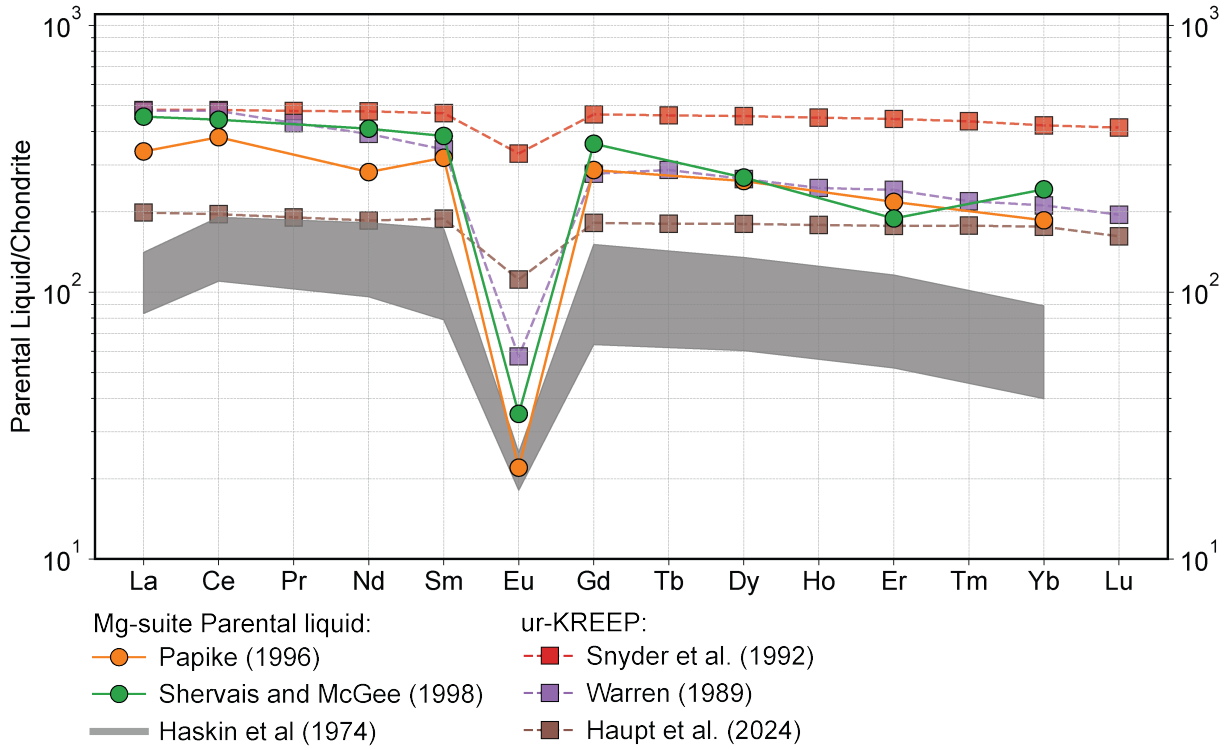

Figure 1. Mg-suite parental liquid REE concentrations estimated by inverting REE data from Mg-suite samples with mineral-melt partition coefficients. These estimations show a clear similarity with the plotted ur-KREEP compositions. However, the phases used in these inversions were likely not liquidus phases and, therefore, reflect the fractioned residual liquid in equilibrium with the measured phase instead of the true Mg-suite parental liquid. Haskin et al., 1974 data are from plagioclase from 76535-21,22, Papike, 1996 data are averages of Apollo 17 norites, Shervais and McGee (1998) data are averages of Mg-suite troctolites from Apollo 17 and 14.

its petrogenesis by trying to reproduce it through the mixing of possible Mg-suite primary parental liquid compositions with modeled ur-KREEP compositions. By constraining the extent of ur-KREEP assimilation, we can improve upon current models of Mg-suite formation, which is a key factor in the internal evolution of the Moon. Importantly, we also demonstrate through this study that geochemical characterization of only a few mineral grains can provide vital information about the petrogenesis of the sample. We therefore present an approach of maximizing scientific output from returned planetary samples in the future, including the Artemis missions.

BACKGROUND - Petrographic and Geochemical Characterization of 76535

Sample 76535 is a 155.5 g troctolite sample collected during a rake. The mineralogy and major element chemistry of 76535 have been extensively described (Dymek et al., 1975; Gooley et al., 1974; Haskin et al., 1974a, 1974b; Bogard et al., 1975; Nord et al., 1976). The mineralogical composition corresponds to 58% plagioclase (An96.2), 39% olivine (Fo87.3), and 2% orthopyroxene (Wo0.9, En84.1, Fs11.3), with trace amounts of clinopyroxene, chromite spinel, apatite, baddeleyite, merrillite, and Fe-Ni alloy. 76535 has a cumulate texture, with the majority of accessory minerals found in mesostasis assemblages. Thermobarometric calculations for 76535 crystallization indicate a 0.2-0.3 GPa and 800-1000 °C cooling regime (Gooley et al., 1974; McCallum and O'Brien, 1996; Schwartz and McCallum, 1999, 2001; White et al., 2020). Borg et al. (2017) used a combination of multiple geochronometers, Sm-Nd, Ar-Ar, and Rb-Sr, and assumed a linear cooling rate to calculate a solidus age of 4384 ± 24 Ma for 76535 and a subsolidus cooling rate of 3.9 °C/Ma. These data are consistent with low-pressure granulite facies metamorphism evidenced by grain annealing and numerous triple-grain junctions. The possible effects of this metamorphism on the chemistry of 76535 will be discussed in greater detail below.

The plagioclase separates from 76535-11 used in this study were previously analyzed for isotopic and bulk chemistry. They were prepared and analyzed by Papanastassiou and Wasserburg (1976) for Rb-Sr and analyzed by Borg et al. (2015, 2017) for Rb-Sr and Sm-Nd systematics. A full description of the preparation of these grains can be found in their work. Briefly, Papanastassiou and Wasserburg (1976) disaggregated the subsample, repeatedly crushed it, and sorted it into mineral separates. During this process, cumulus plagioclase grains, originally ~1 cm (Gooley et al., 1974), were crushed into smaller grains of various sizes. The most important effect of this process on this work is the potential for the analyzed material to contain either core pr rim material or a mixture of both. A determination of the origin of the analyzed grains is included later on.

METHODS

For this study, four plagioclase grain separates from 76535-11 were requisitioned from the Astromaterials Allocation Review Board (AARB). These 1 mm diameter grains (denoted as P-1 to P-4) were mounted in indium and polished using diamond lapping film with 15 and 9 μm grits, followed by powdered diamond abrasives with 3 and 1 μm grits. The chemistry of these mounted grains was then analyzed through an Electron Probe Micro Analyzer (EPMA), Secondary Ion Mass Spectrometry (SIMS), and Laser Ablation Inductively Coupled Mass

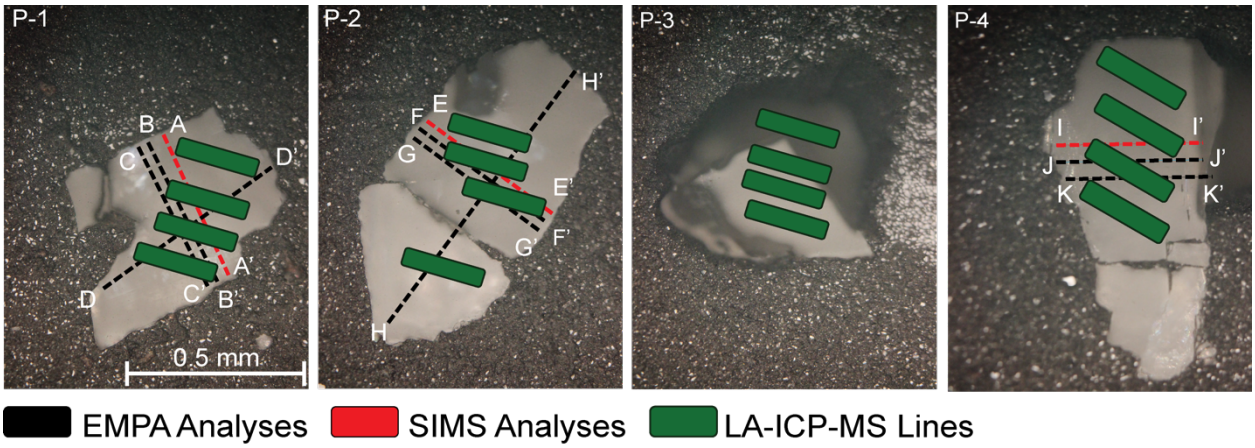

Figure 2. Reflected light photographs of the plagioclase separates with the locations of the different analysis techniques indicated. Grains were polished between analyses to provide adequate surface space for subsequent analyses. Grains P-1 and P-4 show good cleavage into/out of the image plane. However, no systematic chemical variation was observed between P-1/P-4 and P-2/P-3. Letters indicate locations of EPMA (A-A', E-E', and H-H') and SIMS (B-B', C-C', D-D', F-F', G-G', H-H', I-I', and J-J') transects.

Spectrometry (LA-ICP-MS). Complete raw data files from these analyses are available in the supplementary information. Si, Al, Ca, Na, K, Mg, Mn, Fe, Cr, Ti, and Ba concentrations were measured on grains P-1, P-2, and P-4 using a Cameca SX100 EPMA at the University of Arizona Kuiper-Arizona Laboratory for Astromaterials Analysis under the following operating conditions: an accelerating voltage of 15 keV, a beam current of 10-20 nA, and a 5 μm beam diameter. This beam diameter was chosen to limit Na migration during analysis (Kuehn, 2016). The complete list of standards used is provided in the supplemental material., Count times were 10 seconds for Na, Ba, and K and 20 seconds for all other elements. Peak and background counts for individual elements are included in the supplemental materials.

Table 1. 76535-11 Major Element

	P-1	P-2	P-4
SiO_2	43.7±0.4	42.6±0.4	44.3±0.4
Al_2O_3	36±0.5	34.8±0.5	35.9±0.5
MgO	0.09±0.02	0.3±0.03	0.01±0.02
FeO	0.03±0.04	0.12±0.05	0.03±0.04
CaO	19.6±0.2	19.3±0.2	19.4±0.21
Na_2O	0.4±0.08	0.37±0.08	0.47±0.09
K_2O	0.05±0.03	0.05±0.03	0.06±0.03

Measured using EPMA, errors are 2 SD.

Averages of 25 (P-1), 26 (P-2), 23 (P-4) analyses

Table 2. 76535-11 Trace Element from LA-ICP-MS

	P-1	P-2	P-3	P-4
Li 7	2.254±1.756	1.952±1.450	1.940±1.696	2.182±1.336
B 11	1.779±0.270	1.790±0.276	1.722±0.336	1.724±0.294
Sc 45	1.826±0.004	1.829±0.005	1.785±0.004	1.911±0.004
Ti 49	56.997±35.993	77.134±40.896	76.317±46.531	80.311±48.858
V 51*	2.006±0.629	1.994±0.587	1.652±0.401	1.864±0.539
Mn 55*	5.474±0.912	5.610±1.654	5.384±1.262	5.600±0.848
Fe 57*	223.388±75.221	253.978±178.571	216.271±81.562	216.350±39.293
Ni 58*	2.125±6.971	10.566±28.540	1.136±0.440	1.141±0.249
Cu 65*	0.536±0.198	1.055±1.289	0.370±0.210	0.264±0.275
Zn 66*	0.509±0.140	1.326±1.864	0.488±0.179	0.503±0.154
Ga 71*	1.872±0.126	1.877±0.153	1.985±0.167	2.036±0.183
Rb 85*	0.257±0.081	0.301±0.086	0.249±0.057	0.356±0.066
Sr 86*	109.764±6.051	113.016±6.279	112.504±9.469	112.022±9.332
Y 89*	0.962±0.410	1.265±0.537	1.167±0.489	1.247±0.388
Zr 90*	0.344±0.044	1.101±3.653	1.833±3.635	0.361±0.220
Cd 111*	0.035±0.009	0.029±0.010	0.035±0.014	0.053±0.020
La 139‡	1.317±0.163	1.319±0.499	1.267±0.135	1.305±0.157
Ce 140‡	3.533±0.426	3.440±1.204	3.316±0.327	3.573±0.585
Pr 141‡	0.426±0.044	0.399±0.047	0.400±0.035	0.423±0.066
Nd 146‡	1.767±0.207	1.746±0.687	1.676±0.143	1.737±0.341
Sm 147‡	0.423±0.047	0.438±0.206	0.413±0.073	0.424±0.061
Eu 151‡	0.664±0.032	0.646±0.040	0.625±0.039	0.619±0.029
Gd 160‡	0.378±0.056	0.382±0.185	0.381±0.087	0.389±0.042
Tb 159‡	0.054±0.008	0.056±0.029	0.058±0.017	0.057±0.006
Dy 163‡	0.254±0.063	0.265±0.140	0.277±0.081	0.285±0.027
Ho 165‡	0.040±0.015	0.042±0.026	0.045±0.011	0.047±0.006
Er 166‡	0.085±0.034	0.087±0.052	0.098±0.025	0.103±0.013
Tm 169‡	0.007±0.005	0.007±0.005	0.009±0.002	0.009±0.002
Yb 174‡	0.033±0.010	0.096±0.068	0.046±0.012	0.061±0.004
Lu 175‡	0.003±0.002	0.003±0.002	0.004±0.001	0.004±0.001
Pb 208*	0.028±0.006	0.026±0.014	0.029±0.006	0.031±0.011
Th 232*	0.005±0.003	0.004±0.003	0.004±0.003	0.006±0.015
U 238*	0.001±0.001	0.001±0.001	0.000±0.001	0.001±0.008

Analyzed using the X-Series II (unless otherwise indicated)

* Analyzed using the Element™

‡ Analyzed using the Element™ and normalized to Ba

Errors are 2 SD

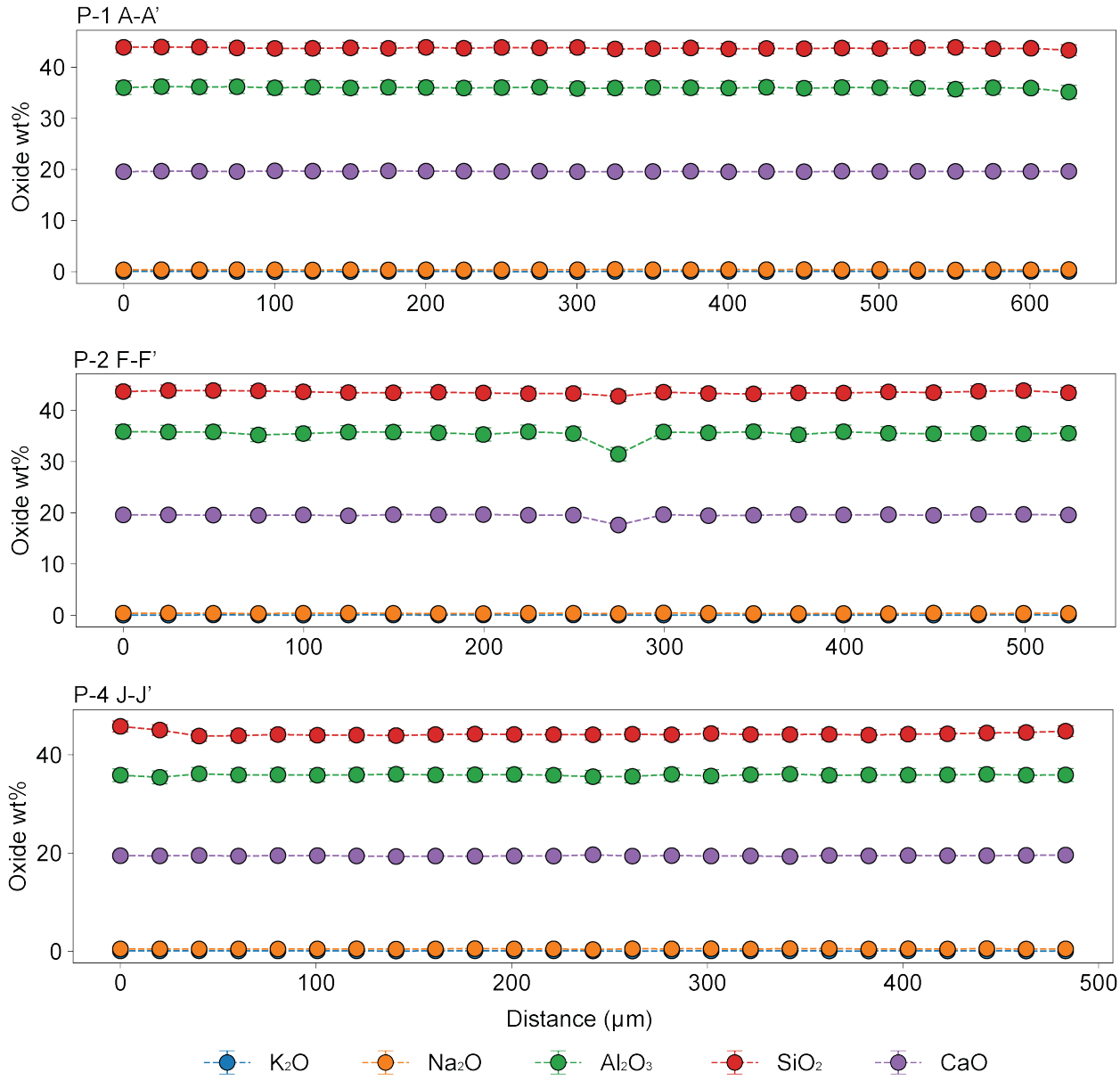

Figure 3. EPMA data from transects of grains P-1, P-2, and P-4. EPMA transects are represented by red lines in figure 1 and are labeled A-A', F-F', and J-J'.

P-2, and P-4 using a Cameca IMS 6f SIMS at Arizona State University's School of Earth and Space Exploration. Calibrations were performed using synthetic NIST glasses (SRM 610, 612, and 614) and natural USGS glasses (GSE-1G, GSA-1G, and GSD-1G). Mg, Ti, K, Fe, and Li, measured with a primary beam current of ~4nA in 20 mu m diameter spots arranged in transects B-B', F-F', and J-J' shown in figure 2. Li, Y, Ba, La, Ce, Nd, Sm, and Eu, measured with a beam current of ~4 nA in 15 mu m diameter spots, analyzed in transects C-C', D-D', G-G', H-H', and K-K'.

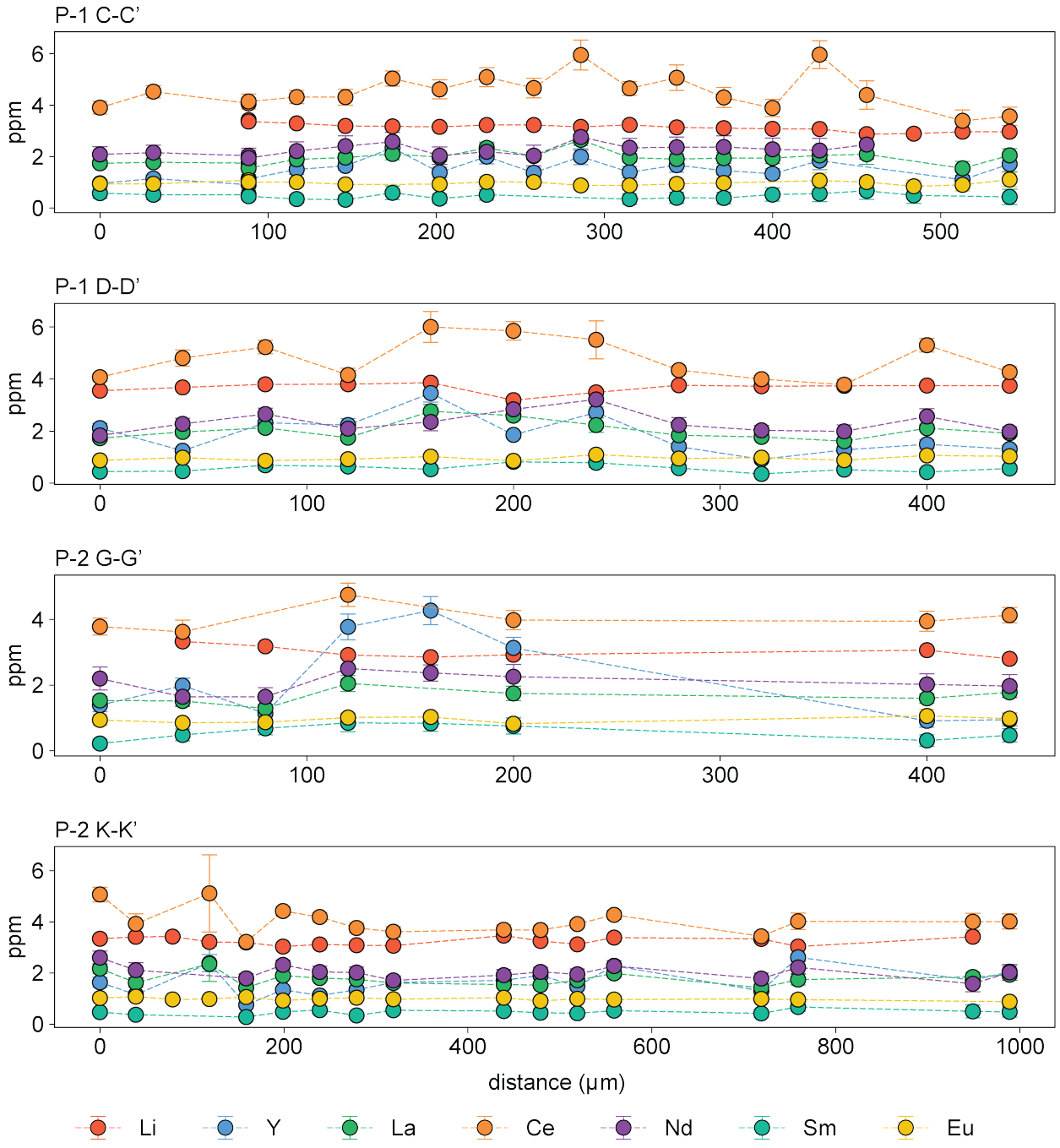

Figure 4. LREE concentrations measured in orthogonal SIMS analysis transects of grains P-1 (C-C', D-D') and P-2 (G-G', H-H'). The location of these transects is shown in figure 1 by black lines. Outliers have been removed based on the Z score and the homogeneity index (discussed further below). The analysis transect of P-4 is available in the supplemental material.

Twenty-nine trace and four minor element concentrations in all four grains were measured by LA-ICP-MS at the University of Arizona geosciences department. Measurements were performed using an Element™ Series high-resolution ICP-MS and an X-Series II multi-collector ICP-MS. Both ICP-MS instruments were coupled to an NWR femtosecond laser with a 100% He

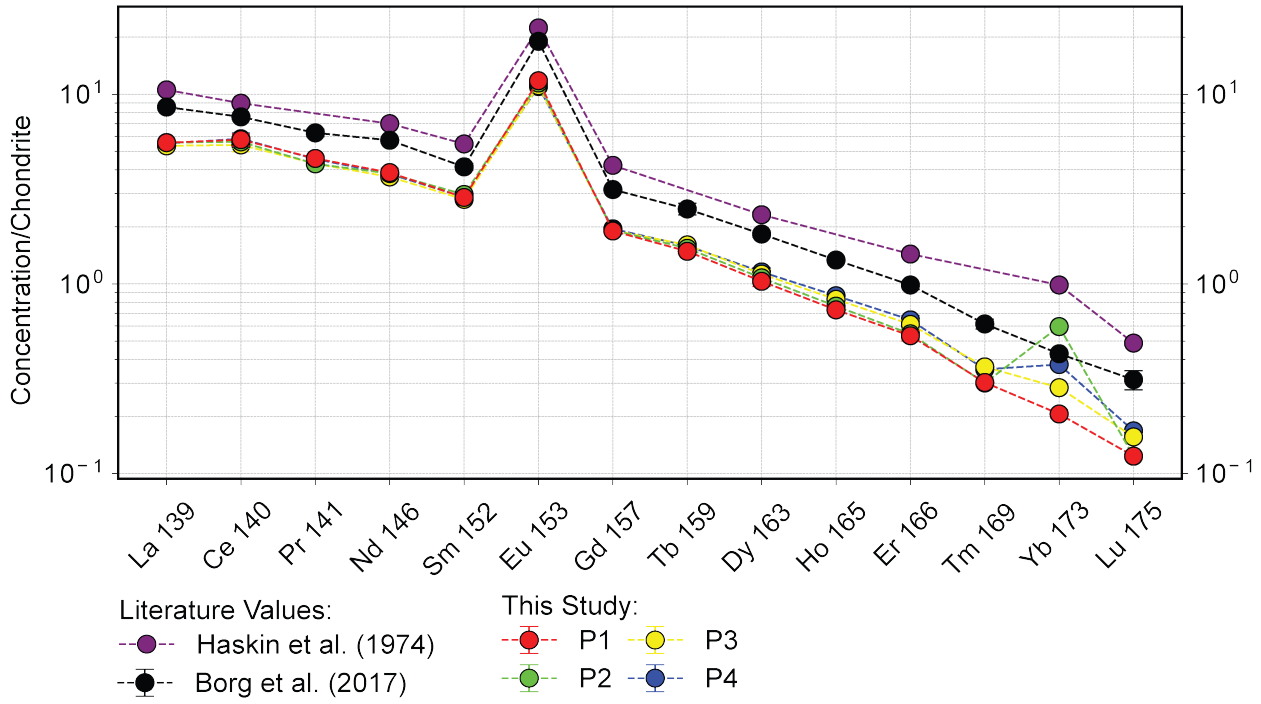

Figure 5. Semi-log plot of REE concentrations of each grain measured on the Element™ high-resolution IC-PMS normalized to chondritic REE values from McDonough and Sun (1995) with 2 SD errors shown. These measurements from this study (P-1, P-2, P-3, and P-4) plot slightly below the solution-based results of Borg et al. (2017) and Haskin et al. (1974). The higher concentrations observed by Borg et al. (2017) and Haskin et al. (1974) may be due to impurities in the digested material., Such impurities may include REE-enriched mineral rims or REE-rich non-plagioclase phases. The positive Yb anomaly may also be due to low total counts and natural abundances of even-numbered Elements.

carrier gas. 4 separate ablations lasting 20 seconds each were conducted on each grain in a series of 300 µm line scans with a 50 μm diameter spot size. Three of the ablations were run at 2.8 $\frac{J}{m^2}$, while the final ablation, which measured the REEs, was run at 7.7 $\frac{J}{m^2}$. A repetition rate of 250 Hz was used for each analysis. Data reductions, including background subtraction, calibration surface creation, and drift corrections, were carried out in Iolite 4™ using the 3D trace element data reduction scheme (Paton et al., 2011; Paul et al., 2023). Trace element yields were normalized to NIST (SRM 616, 614, 612, and 610) and USGS glasses (BHVO, BCR)—a full table of analysis parameters is available in the supplemental materials.

RESULTS

Major and minor element analyses were completed on the plagioclase grain separates. Analytical results for major elements of grains P-1, P-2, and P-4, as measured by EMPA, are reported in table 1 and figure 3. The average An content of the three measured grains is 97.6 ± 6, which is consistent with previous measurements of 76535 plagioclase (Haskin et al., 1974; Borg et al., 2017) and plagioclase within the wider Mg-suite (Shearer et al., 2015). Minor element measurements from EMPA and SIMS (table 1 and figure 4) are in good agreement.

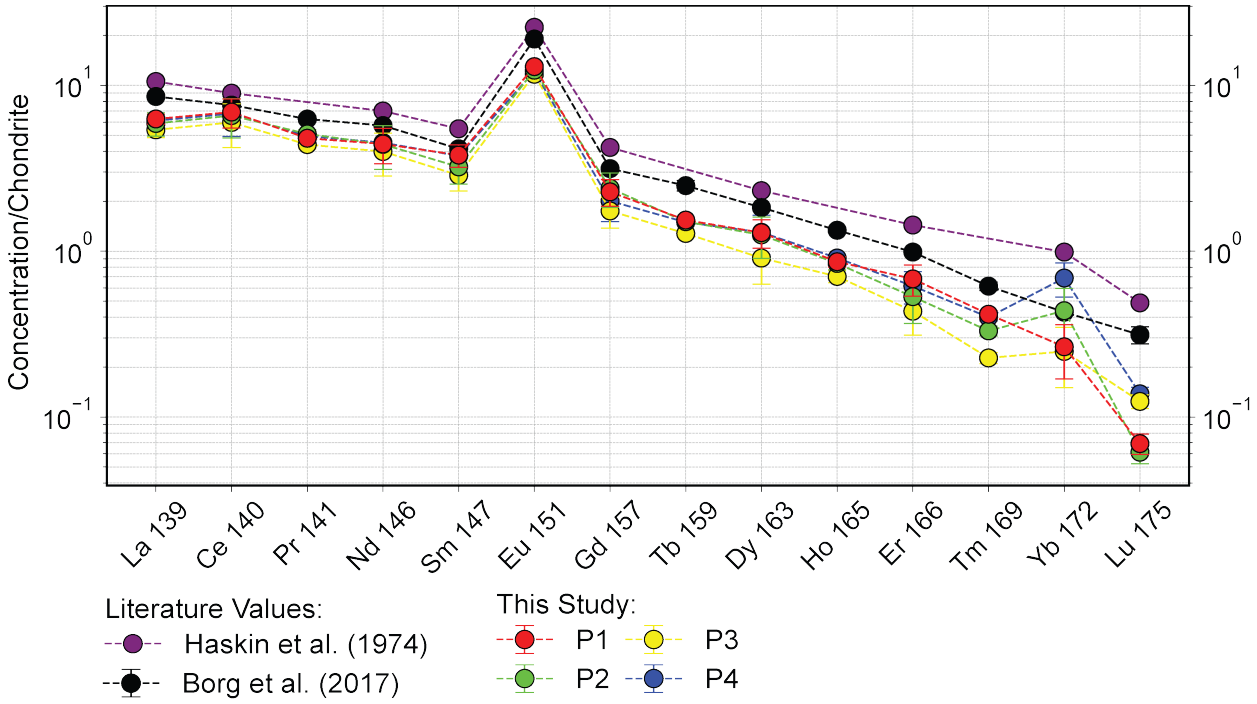

Figure 6. Semi-log plot of REE concentrations of each grain measured on the X-Series II multi-collector ICP-MS normalized to chondritic REE values from McDonough and Sun (1995) with 2 SD errors shown. These measurements, like those made by the Element™ plot slightly below the solution-based results of Borg et al. (2017) and Haskin et al. (1974).
Figure 7. Estimated diffusion profiles between plagioclase and olivine calculated at constant Nd diffusivity plotted at 5 Ma intervals. Diffusion profiles extend a maximum of 300 \mu m into the plagioclase grains. This diffusion profile calculated using the chosen Nd diffusivity of $1.12 \times 10^{-23}\ m/s^2$, which corresponds to 900 °C and An93, represents an upper bound on possible diffusive profiles. The SIMS analysis transects for P-1 (C-C' and D-D') are also plotted to show the inconsistency of the measured concentration topography with the predicted diffusion profiles.

The results of the SIMS transects are recorded in figure 4. Measurements for both groups of elements were normalized to the counts of Si, and a correction for BaO interference with Eu was applied (Hinton, 1990). Because the chemistry of the plagioclase crystals does not change (relative to the uncertainty of analysis) across the grain, we would label the crystals as homogeneous. Because the grains are not in situ, their rims cannot be identified with certainty. Nevertheless, the fact that all grains are compositionally consistent across their surfaces implies minimal zoning in the sample and supports the interpretation that the material measured for this work comes from grain cores. The quantification of this homogeneity in LREEs will be discussed later on.

The results of the LA-ICP-MS are shown in table 2. These analyses reveal enrichments in LREEs between 1- and 10-times chondritic values. HREEs are depleted by about 0.1 times relative to chondrites. The SIMS and LA-ICP-MS analyses deliver similar abundances for Ba, Sr, and Y. The increased counts on the LA-ICP-MS allow for better, higher precision measurements of HREEs, which range from ~3 to ~400 ppb. The positive Yb anomaly seen in P-

2, P-3, and P-4 may be an artifact of the low total counts for individual HREEs and the naturally more abundant even-numbered elements. Notwithstanding, the La/Yb ratio of the samples ranges from 10 to 30, consistent with previous measurements of 76535 plagioclase (Haskin et al., 1974; Borg et al., 2017). The solution-based ICP-MS of 76535-11 by Borg et al., 2017 is also reported in figures 5 and 6. The separation of the HREE data from Borg et al. (2017) and that of this study may arise from impurities within the mineral separates and the mixture of grain cores and rims, which may have different REE concentrations in the dissolved material for the solution-based methods, highlighting the importance of in-situ characterization over bulk characterization in this context.

DISCUSSION

Determining the petrogenesis of the Mg-suite requires an accurate characterization of its parental liquid. Fixing the parental REE composition allows us to evaluate the hypotheses that ur-KREEP material contributed to the petrogenesis of the Mg-suite. The inversion method used by previous studies for estimating REEs in the Mg-suite parental liquid estimate the concentrations of the residual liquid at the point on the liquid line of descent where the analyzed material was on its liquidus. To accurately assess the potential for ur-KREEP assimilation, the 'true' parental liquid of Mg-suite magmas is needed.

To this end, a Python-based forward model was created, which utilizes a modeled Mg-suite liquid line of descent (LLD). The accuracy of this forward model relies on first determining that the sample preserves its magmatic chemistry (Shervais and McGee, 1998). We present here two lines of evidence that support the assumption that the REE measurements we performed are representative of magmatic conditions. The first is the statistical quantification of the homogeneity of these grains, as revealed by the SIMS analysis transects. The second is a calculation of diffusive profiles within plagioclase, which explores possible subsolidus diffusion of REEs.

Grain Homogeneity

A significant advantage of our microanalysis studies is the ability to detect intragrain heterogeneity at a scale of a few tens of microns, which is not achievable with solution-based analyses. Characterizing the homogeneity of REEs within 76535 plagioclase serves to increase the confidence of our measured REE values as it provides a criterion to reject anomalous measurements. Additionally, a homogeneous sample will be free from concentration gradients, the products of slow crystallization or subsolidus diffusion. Both of these effects serve to increase the confidence of our modeled parental liquid.

Quantifying a sample's homogeneity requires distinguishing the effects of the measurement uncertainty from true compositional variations within the material., Harries (2014) presents a model to estimate the contribution of compositional heterogeneity S_h and measurement uncertainty (S_{rms}) to the combined uncertainty budget (S_c) of geologic reference materials. This model creates a statistically sound method for quantifying the homogeneity of the sample through a homogeneity index (H) and F statistics. Equation 1 shows the relationship presented by Harries (2014), where S_c

$$H = \frac{E(S_c)}{E(S_{meas})} \approx \frac{S_c}{S_{rms}} \quad (1)$$

Table 3. Homogeneity Indices

P-1 (N = 31)	S_{rms}	S_c	H	$F^{1/2}$	Test Passed
Li	0.283	0.308	1.09±0.14	1.298	YES
Y	1.867	0.644	0.34±0.04	1.298	YES
Ba	8.827	1.801	0.20±0.03	1.298	YES
La	1.242	0.394	0.32±0.04	1.298	YES
Ce	2.397	0.889	0.37±0.05	1.298	YES
Nd	2.246	0.381	0.17±0.02	1.298	YES
Sm	1.305	0.174	0.13±0.02	1.298	YES
Eu	1.027	0.085	0.08±0.01	1.298	YES
P-2 (N = 28)	S_{rms}	S_c	H	$F^{1/2}$	Test Passed
Li	0.242	0.243	1.00±0.13	1.284	YES
Y	2.282	1.004	0.44±0.06	1.284	YES
Ba	7.427	0.688	0.69±0.09	1.284	YES
La	1.347	0.462	0.34±0.05	1.284	YES
Ce	2.672	1.096	0.41±0.05	1.284	YES
Nd	2.157	0.445	0.21±0.03	1.284	YES
Sm	1.211	0.218	0.18±0.02	1.284	YES
Eu	0.757	0.125	0.15±0.02	1.284	YES
P-4 (N=6)	S_{rms}	S_c	H	$F^{1/2}$	Test Passed
Li	0.309	0.237	0.77±0.24	1.737	YES
Y	2.732	0.913	0.33±0.11	1.737	YES
Ba	9.557	2.302	0.24±0.08	1.737	YES
La	2.537	0.732	0.29±0.09	1.737	YES
Ce	6.290	1.571	0.25±0.08	1.737	YES
Nd	3.896	0.784	0.20±0.06	1.737	YES
Sm	1.469	0.204	0.14±0.04	1.737	YES
Eu	0.938	0.176	0.19±0.06	1.737	YES
Combined	S_{rms}	S_c	H	$F^{1/2}$	Test Passed
Li	0.264	0.331	1.25±0.11	1.204	NO
Y	2.100	0.851	0.41±0.04	1.204	YES
Ba	8.180	3.655	0.45±0.04	1.204	YES
La	1.408	0.459	0.33±0.04	1.204	YES
Ce	2.954	1.051	0.36±0.03	1.204	YES
Nd	2.344	0.449	0.19±0.02	1.204	YES
Sm	1.259	0.195	0.16±0.01	1.204	YES
Eu	0.926	0.116	0.12±0.01	1.204	YES

Errors on H values are minimum uncertainty of H calculated following methods in Harries (2014).

root mean square of the uncertainties of the mass fractions. A homogeneous material will, therefore, return an H value of ~1. The homogeneity index (H) is the square root of a variance ratio, and it follows, therefore, that H^2 is a variance ratio that can be used to test the null hypothesis shown in equation 2. In this hypothesis, $E(S_c)$ represents the expected variance of the combined uncertainty, and

$$E(S_c^2) = E(S_{meas}^2) \quad (2)$$

$E(S_{meas})$ is the expected variance due to measurement uncertainty. Equation 3 outlines the F-test used to calculate the probability of rejecting the null hypothesis. $F_{(\alpha,\upsilon_1,\upsilon_2)}$ is the critical F value which incorporates the degrees of freedom of S_c and S_{rms}, υ_1 = N-1 and υ_2 = infinity respectively. The

$$H^2 > F_{(\alpha,\upsilon_1,\upsilon_2)} \quad (3)$$

significance level alpha was set at 0.01, corresponding to the probability of falsely rejecting the null hypothesis (considering a homogeneous material heterogeneous).

Failing to reject the null hypothesis in this test boosts our confidence in the spatial homogeneity of the sample. This outcome also provides a basis for dismissing outlier values as unrepresentative. The calculations of the homogeneity index and the subsequent F test using the SIMS transect data are detailed in table 3. The analyzed grains contain no detectable heterogeneity, with the majority of H values being <1. Additionally, we calculated a homogeneity index for the combination of the three grains, which revealed measurable inter-grain heterogeneity in lithium only. The observed high inter-grain (excluding Li) and intra-grain homogeneity align with previous assessments of mineral chemistry in sample 76535 (Haskin et al., 1974). In the absence of complete diffusive homogenization, this result suggests that the measured REE concentrations accurately reflect the magmatic concentrations of the parental liquid at the time of crystallization. In the following section, the potential for diffusive homogenization is explored.

Subsolidus Diffusion of Trace Elements

The slow cooling and granoblastic texture of the original 76535 plagioclase necessitates consideration of subsolidus diffusive processes to assess the suggestion that the measured trace element concentrations reflect plagioclase-magma equilibrium conditions (Shervais and McGee, 1998; Warren et al., 1993). Given the nature of the plagioclase separates it is possible that the material measured for this work, represents entirely grain core or rim material, or a mixture of both. To this end, we employed a one-dimensional diffusion model that simulates the migration of Nd from plagioclase into neighboring olivine. Our objective with this exercise is to define a possible Nd diffusion profile within a hypothetical 76535 plagioclase and compare those estimates to the topography of Nd concentrations in the SIMS analysis transects. The result of this exercise will be determining whether the measured material is grain core material, and the extent that that Nd has been affected by diffusion. Given their limited range of ionic radii, the result of this exercise is expected to be applicable to all REEs, not just Nd. The model utilized a one-dimensional, non-steady-state diffusion framework, treating the plagioclase and surrounding olivine as discrete segments, with Dirichlet boundary conditions applied at both ends. Diffusion was modeled using an analytical solution to Fick's Second Law (Mehrer, 2007) shown in equation 4, where c_1 and c_2 denote the concentrations in plagioclase and olivine, respectively, D represents the diffusivity of Nd in plagioclase, and t represents time in millions of years.

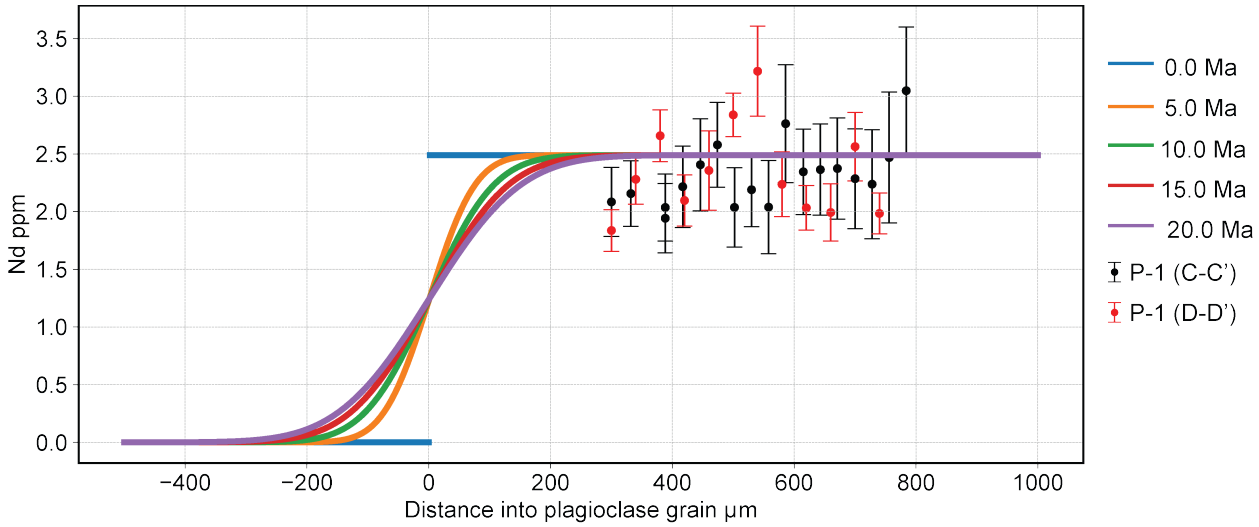

Figure 7. Estimated diffusion profiles between Plagioclase and olivine calculated at constant Nd diffusivity plotted at 5 Ma intervals. Diffusion profiles extend a maximum of 300 \mu m into the plagioclase grains. The chosen Nd diffusivity of $1.12 * 10^{-23}$ m^2/s corresponds to 900 °C and An93 represents an upper bound on possible diffusive profiles. The SIMS analysis transects for P-1 (C-C' and D-D') are also plotted to show the inconsistency of the concentration topography with the predicted diffusion profiles.

$$c(x,t) = \frac{(c_2 - c_1)}{2}\left(1 + \text{erf}\left(\frac{x}{2\sqrt{Dt}}\right)\right) \quad (4)$$

The initial Nd of plagioclase in the model was set at 2.615 ppm, the Nd measured in 76535-11 plagioclase by Borg et al., 2017 and the initial Nd in olivine was 0.125 ppm as measured in 76535, 21-22 by Haskin et al., 1974. The Nd diffusivity used in this model was calculated for An93 at 900 °C using the Arrhenius relation outlined in equation 4 (Cherniak et al., 2003), where R represents the gas constant $\left(8.314 \times 10^{-3}\ \frac{kJ}{mol} \cdot K\right)$ and T is the temperature in Kelvin.

Diffusivity in plagioclase

$$D = 5.9 * 10^{-6} \exp\left(\frac{-398}{RT}\right) \quad (5)$$

is inversely. Correlated with both temperature and calcium content (Cherniak et al., 2003), therefore holding diffusivity constant at $1.12 \times 10^{-23}\ \frac{m}{s^2}$, the value corresponding to 900 °C for An 93, estimates an upper limit for potential diffusion in the An 97 plagioclase from 76535. Diffusion was modeled this way over 20 Ma, consistent with the subsolidus cooling rate of 3.9 $\frac{^\circ C}{Ma}$ defined by Borg et al. (2017) from the solidus at approximately 900 °C, as determined by RhyoliteMELTS (Gualda et al., 2012; Ghiorso et al., 1995; Asimow and Ghiorso, 1998), to the closure temperature of Nd in Plagioclase around 825 °C, (Borg et al., 2017). The modeled diffusion profiles generated from this solution are presented in figure 7. The modeled diffusion profiles after 20 million years extend a maximum of 300 μm into the plagioclase grains, with pronounced diffusion occurring near the grain edges. This diffusion creates a profile that matches

Na kα X-ray intensity maps of 76535-55 plagioclase (Nelson et al., 2021) and 14321 (Shervais and McGee, 1998) and would be detectable with the analytical precision of the SIMS. The SIMS analyses transects revealed no core-to-edge diffusive profiles or noticeable heterogeneity, suggesting that the measured REE concentrations sample the core of original plagioclase grains and represent magmatic conditions. The absence of observable diffusion profiles suggests that the material sampled in this study originated from the core of cumulus plagioclase grains. Therefore, we feel confident in the assumption that the measured concentrations of Nd and other REEs are magmatic.

Estimating Parental Melt Composition

We estimated the unfractionated Mg-suite parental liquid using a Python-based forward model. This model relies on a modeled LLD created using the thermodynamic code RhyoliteMELTS 1.0.2 (Gualda et al., 2012, Ghiorso et al., 1995; Asimow and Ghiorso, 1998). The LLD was calculated using a potential Mg-suite parental liquid major element composition first proposed by Longhi et al., 2010 and adapted by Prissel et al., 2016 as a starting liquid, which was then fractionally crystallized from the liquidus at approximately 1544 °C to 900 °C. This major element composition was selected because it has been shown to reproduce the mineralogy of the Mg-suite troctolites (Prissel et al., 2016). RhyoliteMELTS-defined LLD provides the mass fraction and composition of Minerals being fractionated from the starting liquid at each temperature step. The pressure for these calculations was set at 0.26 GPa, consistent with available Thermobarometric data (Gooley et al., 1974; McCallum and O'Brien, 1996; Schwartz and McCallum, 1999, 2001; White et al., 2020). The forward model then ascribes an initial guess for each REE to the starting liquid, which is then fractionated into each phase as it forms based on the calculated mineral-melt partition coefficient for spinel, olivine, plagioclase, orthopyroxene, and clinopyroxene. The methods for calculating these partition coefficients are detailed in the following sections. The forward model, therefore, produces a set of fractionated minerals with their equilibrium REE content at each temperature step along the LLD. The initial guess of each REE in the parental liquid was then varied until a plagioclase with REE concentrations matching those measured in the 76535 plagioclase was fractionated within a target temperature window (1244 °C -1256 °C). The target temperature window was determined as the range of temperature where the fractioned mineral most closely matched the modal mineralogy of 76535. The input files used in calculating the LLD RhyoliteMELTS input and output files are included in the supplemental materials available on ReData (See Appendix B). The method for calculating the unfractionated parental liquid is outlined in figure 8 and the results of this forward model are shown in figure 9.

This exercise reveals a parental liquid with a strong resemblance to calculated ur-KREEP compositions, being enriched to 100s of times chondritic values with a decreasing trend towards HREEs. Additionally, inversion was used to estimate the fractionated parental liquid when plagioclase was on the liquidus using the data from this study along with data from Borg et al. (2017), Haskin et al. (2017), and Shervais and McGee (1998). The plagioclase-melt partition coefficients for these inversions were calculated at 1271 °C; the temperature that plagioclase appears on the liquidus, as defined by RhyoliteMELTS. These fractionated liquids, plotted in figure 9, show additional enrichments in REEs. Finally, we inverted the 78235 norite plagioclase compositions from Papike (1996) which is more enriched still. These estimates and the unfractionated parental liquid may represent various points along the crystallization of a single

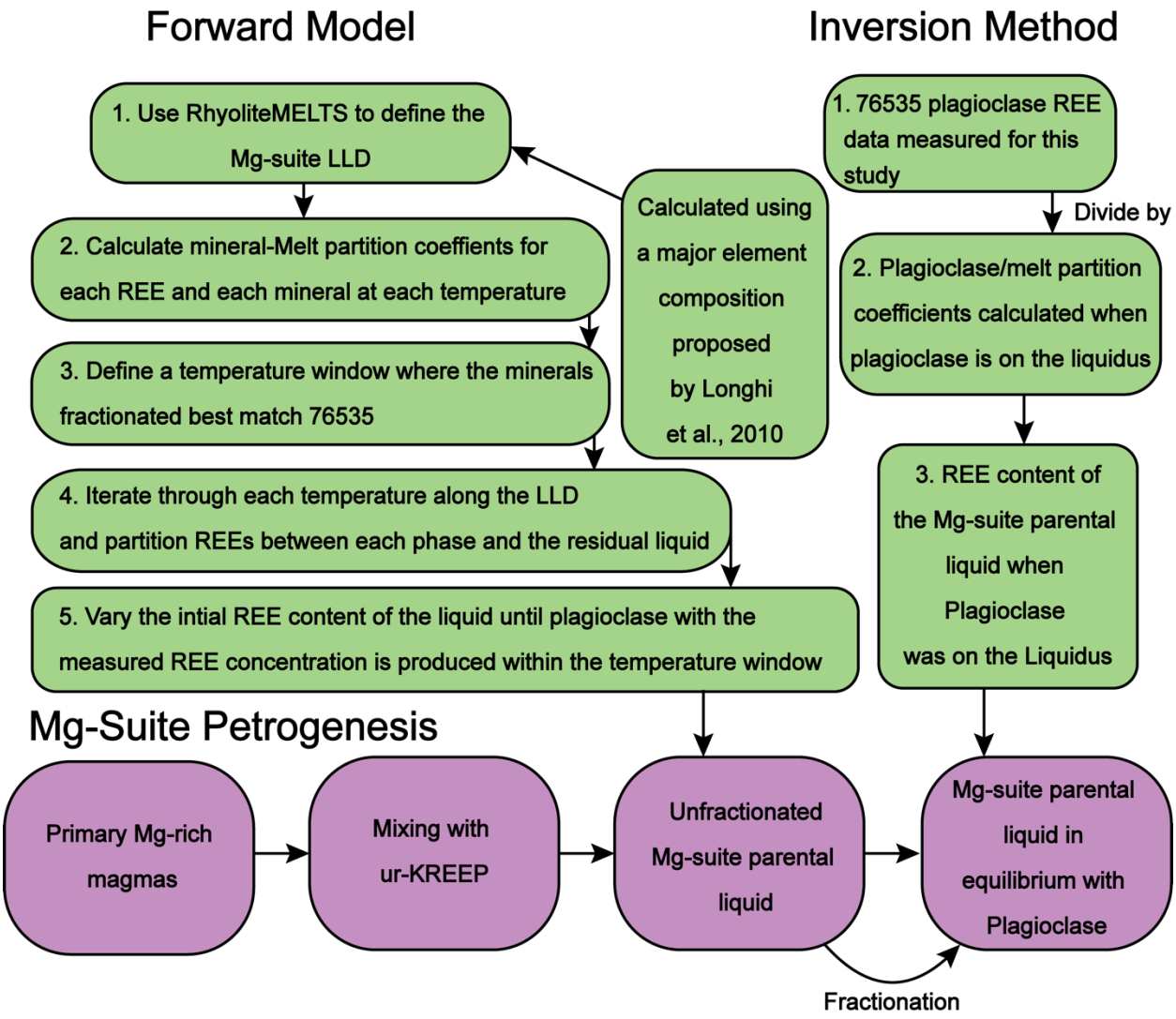

Figure 8. Flow chart outlining the process of calculating the unfractionated parental liquid through the forward model and inversion. Green squares represent the processes involved in estimating the parental liquid and the purple squares shows where in the petrogenesis of the Mg-suite these estimated liquids fit.

magma. Now that we are confident in the accuracy of our estimated parental liquid composition, we explore the petrogenesis of the Mg-suite and assess the extent of ur-KREEP assimilation.

Mineral-melt Partition coefficients

Partition coefficients between the phases of the RhyoliteMELTS-defined LLD and the residual liquid are required to recreate the parental liquid. These coefficients, representing the expected concentration ratio of an element between two phases, can be sensitive to various factors and have been the topic of extensive experimental investigations. Previous estimates of the Mg-suite parental liquid used a range of published partition coefficients to invert measured sample REE data (Haskin et al., 1974; Papike 1996; Shervais and McGee, 1998; shown in figure 1) The

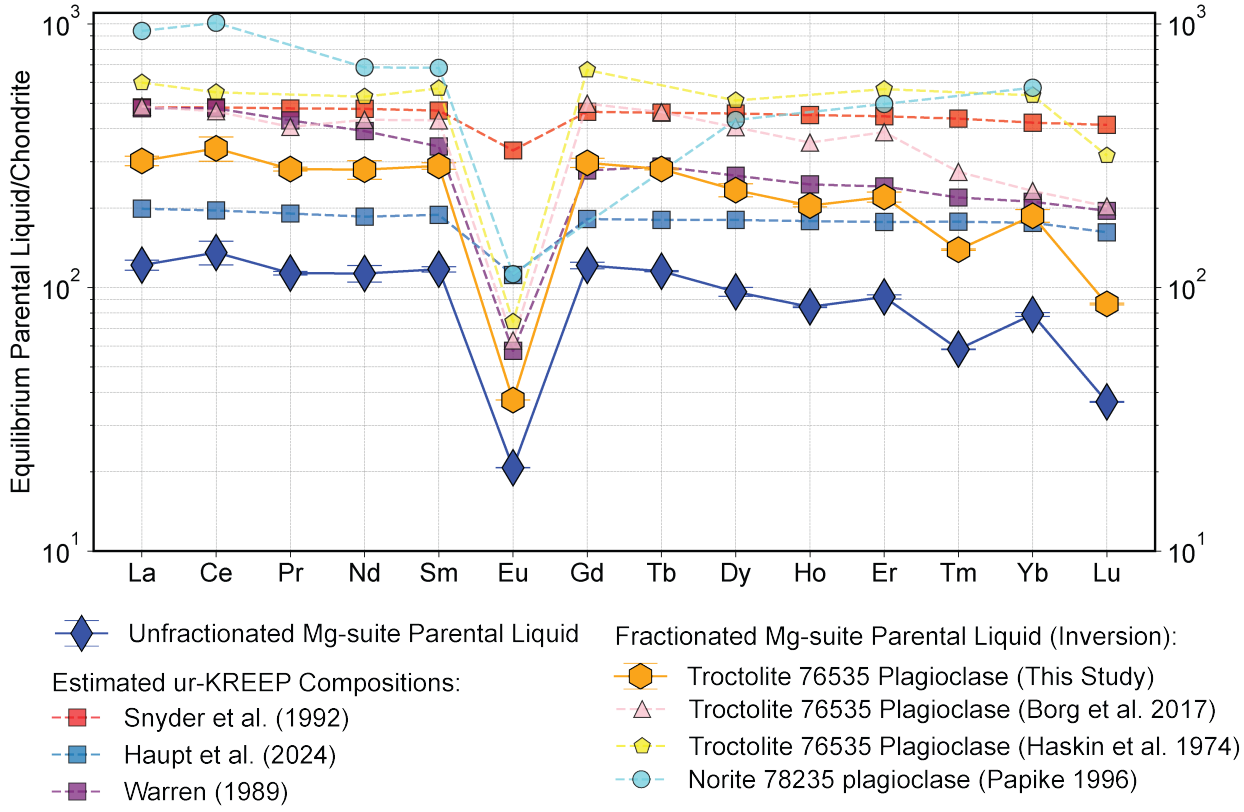

Figure 9. Semi-log plot of the estimated parental liquids normalized to chondritic REE values from McDonough and Sun (1995). Errors on parental liquids from this study are two standard error, calculated through a Monte Carlo simulation following the methods of Anderson, 1976. For most points, the errors are too small to see at this scale. Ur-KREEP compositions are plotted as squares to distinguish them from estimated parental liquids.

parental liquid in both the inversion methods and the forward model presented in the previous section are highly sensitive to the partition coefficient values, necessitating careful consideration of how the values are determined.

The partition coefficients for olivine, orthopyroxene, clinopyroxene, and plagioclase were calculated using the lattice strain model proposed by Blundy and Wood (2003) shown in equation r. In this

$$D_{\mathrm{REE}}^{\text{min-melt}} = D_0 \exp\left[\frac{-4\pi E N_A}{RT}\left(\frac{r_0}{2}\left(r_0 - r_j\right)^2 - \frac{1}{3}\left(r_0 - r_j\right)^3\right)\right] \quad (6)$$

model, D_0 represents the strain-free partition coefficient, r_0, the strain-free lattice site ionic radius, and E_0, the effective Young's modulus of the crystal lattice. Parametrization of these variables for olivine, orthopyroxene, and clinopyroxene was calculated through regression of existing experimental data by Sun et al. (2014). The pressure for the partition coefficient calculations was likewise set at 0.26 GPa, consistent with available Thermobarometric data (Gooley et al., 1974; McCallum and O'Brien, 1996; Schwartz and McCallum, 1999, 2001; White et al., 2020). A similar parametrization for plagioclase was performed by Sun et al. (2017), which incorporates experimental data produced by Sun et al., using lunar magma compositions. These parameterizations have been shown to fit the available experimental data at a range of

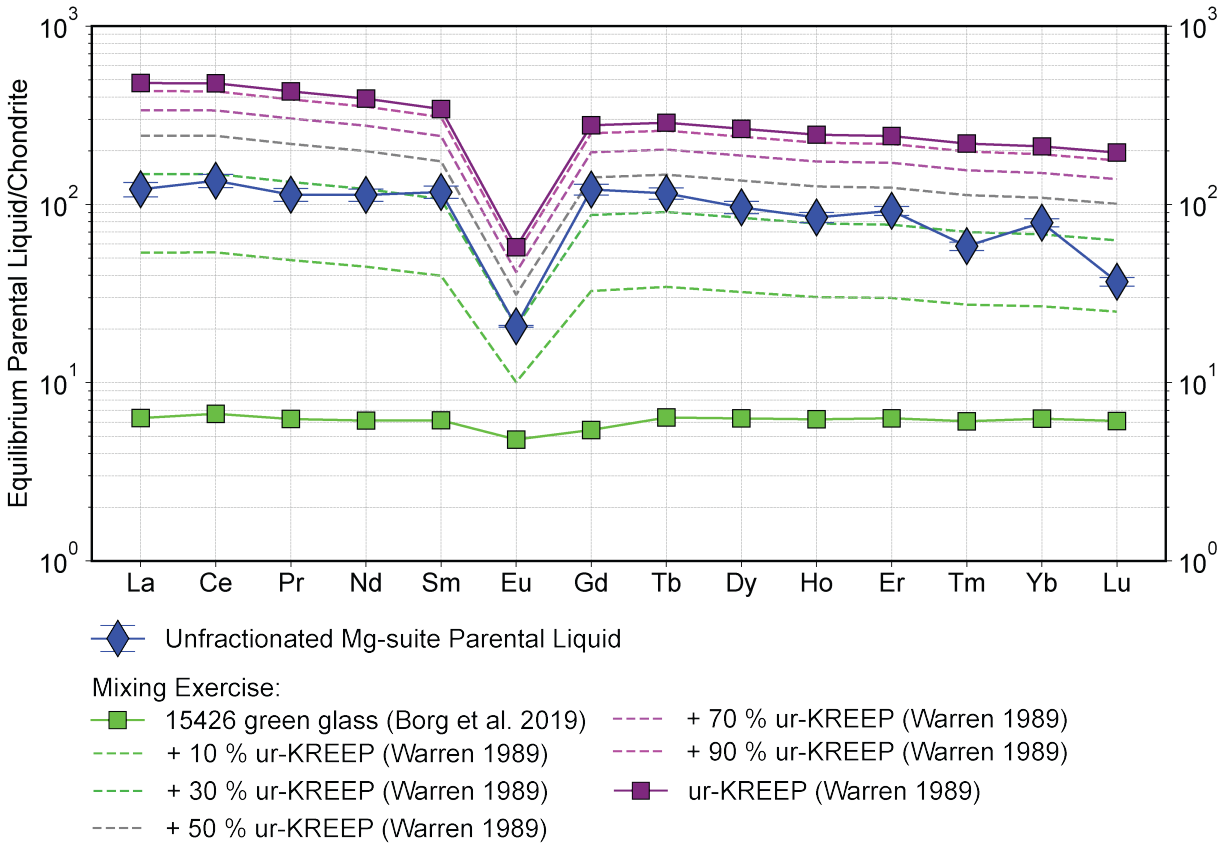

Figure 10. Semi-log plot showing the mixing exercise between the 15426 green glass (Borg et al., 2019) and the ur-KREEP concentration modeled by Warren et al., 1989 in comparison to the estimated Mg-suite parental liquid, both normalized to chondritic REE values from McDonough and Sun (1995). In this scenario, the ur-KREEP concentrations are more enriched in LREEs, similarly to the estimated parental liquid, negating the need for additional alteration of REEs with the parental liquid.

pressure, temperature, and liquid composition. No parametrization currently exists for spinel REE partitioning, so experimental values from (Irving, 1978) were used. Although the spinel partition coefficients are not as well constrained compared to the other phases, their effect on the estimated parental liquid is minimal due to the small mass fraction of spinel. These improved partitioning values, along with the high pristinity of 76535, the high homogeneity of the sample, and the high quality of our measurements, lend themselves to the estimation of a high-fidelity parental liquid composition.

Mg-suite Petrogenesis

Considering the high homogeneity and limited diffusion of REEs within 76535 plagioclase, and the strong KREEP signature of the estimated parental liquid, we suggest that a signification ur-KREEP contribution to the Mg-suite primary parental liquid is expected. This evidence, in combination with the previously presented chronological data leads us to propose the following model for Mg-suite formation: (1) FAN crystallization and ur-KREEP segregation at 4359 ± 9 Ma (Borg et al., 2017) and 4368 ± 29 Ma (Gaffney and Borg, 2014; Snape et al., 2016;

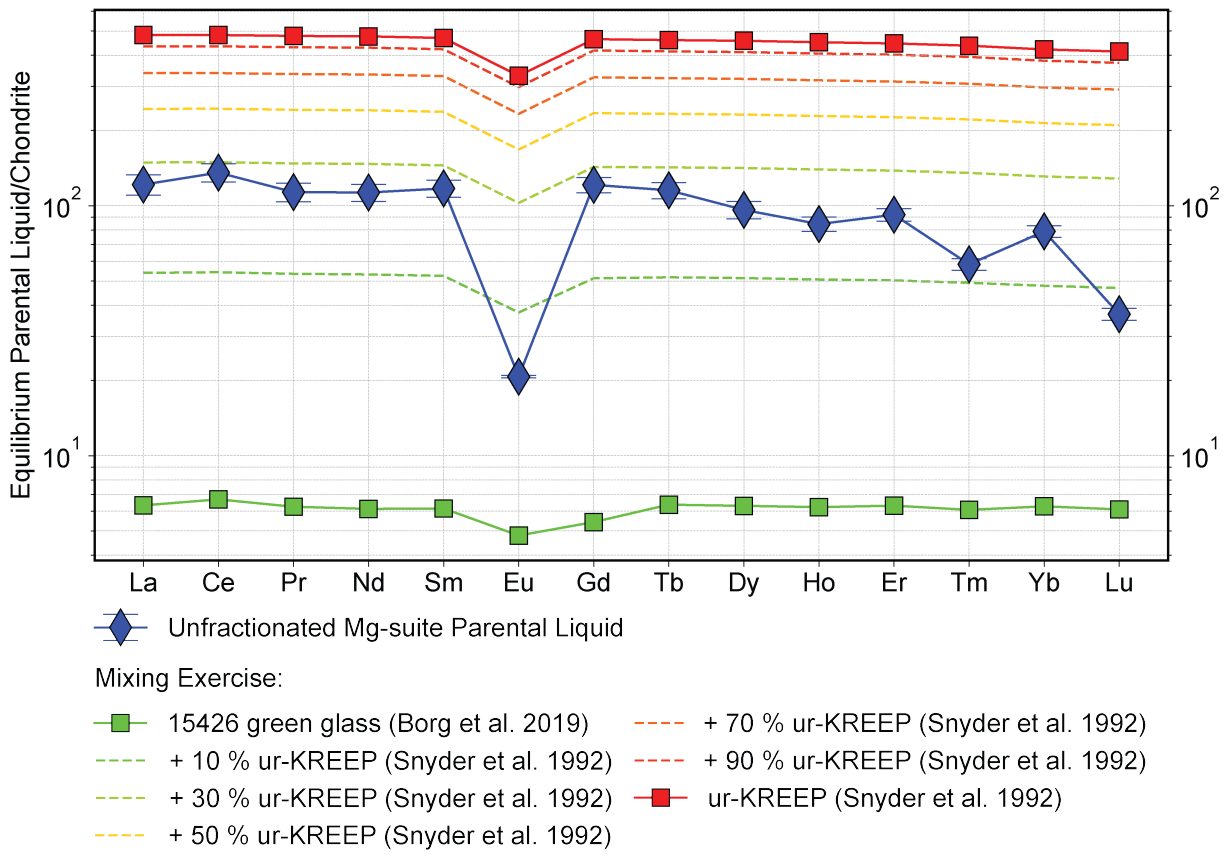

Figure 11. Semi-log plot showing the mixing exercise between the 15426 green glass (Borg et al., 2019) and the ur-KREEP concentration modeled by Snyder et al., 1992 in comparison to the estimated Mg-suite parental liquid both normalized to chondritic REE values from McDonough and Sun (1995). The HREE depletion in the parental liquid, cannot be explained by this mixing exercise alone and may require the fractionation of an HREE-rich phase which is explored in Figure 12.

and Maurice et al., 2020) respectively, (2) formation of the primary Mg-suite melt through decompression of rising magma ocean cumulates at 4345 ± 10 Ma (Borg et al., 2020), (3) assimilation of ur-KREEP material by the primary Mg-suite melt, leading to REE enrichment and formation of unfractionated parental liquid of Mg-suite; (4) fractionation of the parental liquid, and emplacement into the lunar crust. This petrogenetic model explains Cr-spinel bearing troctolites, whereas pink spinel troctolites or anorthosites require additional steps i.e. reaction of the parental liquid with crustal wall rock (Prissel et al., 2016 and Sheikh et al., 2024). The final objective of this work is to constrain the extent to which ur-KREEP material contributed to the Mg-suite primary parental liquid.

To this end, mixing exercises were conducted between different estimated ur-KREEP compositions (Haupt et al., 2024; Warren et al., 1989, and Snyder et al., 1992) and a potential primary Mg suite liquid. The REE compositions for potential Mg-suite primary parental melt were taken from 15426 green glass beads (Borg et al., 2019), which are believed to be among the

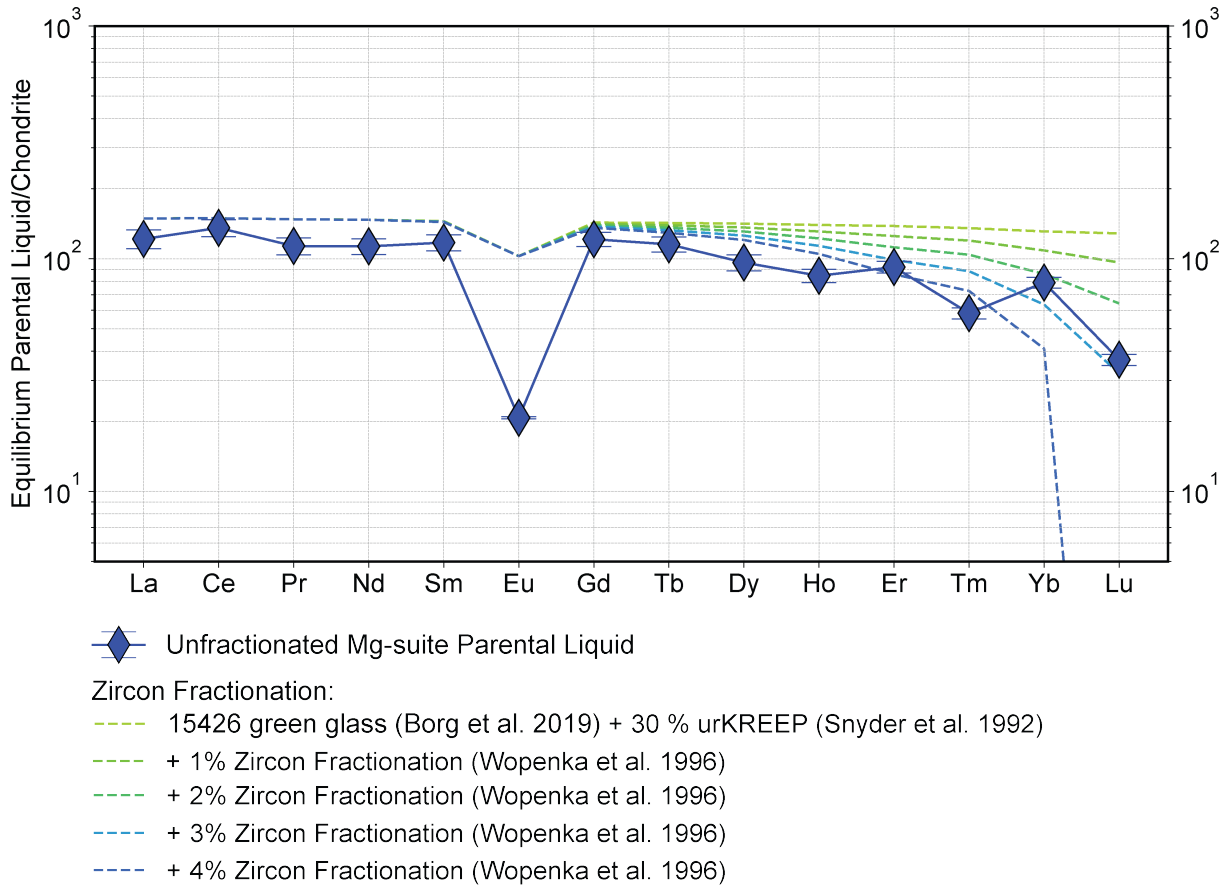

Figure 12. Semi-log plot simulating the fractionation of a lunar zircon Composition (Whitehouse and Nemchin, 2009) from a mixture of the 15426 green glass (Borg et al., 2019) and the ur-KREEP concentration modeled by Snyder et al., 1992 compared to the estimated Mg-suite parental liquid normalized to chondritic REE values from McDonough and Sun (1995). In this exercise, zircon represents a range of possible HREE-rich phases identified in 76535 and other Mg-suite samples, which include baddeleyite, merrillite, and zircons.

most primitive lunar volcanic rocks sampled thus far (Tatsumoto et al., 1987). These mixing exercises suggest that reproducing the estimated parental melt requires a 30-50% ur-KREEP contribution. The results of mixing ur-KREEP compositions from Warren (1989) and Snyder et al. (1992) are shown in figures 9 and 10, while the remaining mixing combinations are reported in the supplemental material.,

Some of the estimated ur-KREEP compositions contain flat REE trends (Snyder et al., 1992 and Haupt et al., 2024), which, in combination with the flat green glass trends (excluding Eu) (figures 10 and 11), cannot fully explain the REE composition of the estimated Mg-suite parental liquid. Thus, a two-stage model for Mg-suite petrogenesis may be necessary. This model would contain, first, a mafic primary melt that assimilates ur-KREEP material, and second, the fractionation of HREE-rich phases. This HREE depletion through fractionation was explored in a second mixing exercise. Figure 12 shows the results of zircon fractionation from a mixture of

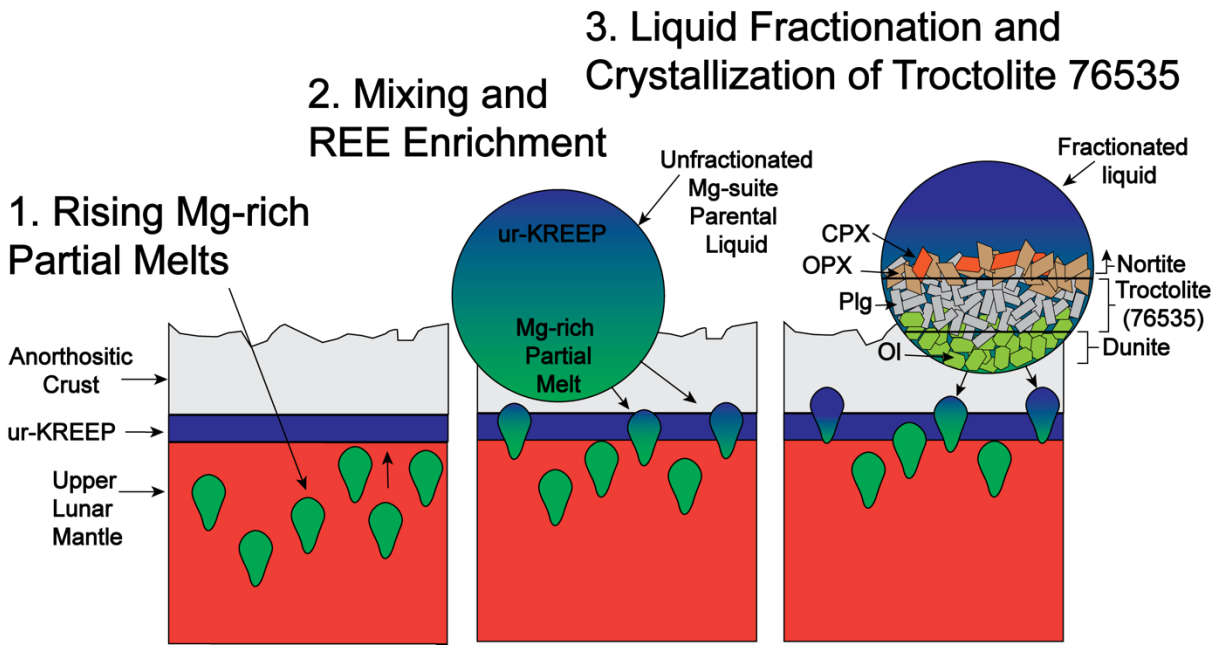

Figure 13. Cartoon which demonstrates the outlined model for Mg-suite petrogenesis. In the first section, rising mafic cumulates are partially melted and come into contact with ur-KREEP in the upper mantle. These lithologies then mix in the second section, enriching the REE concentrations of the newly formed Mg-suite parental liquid. After this point the Mg-suite parental liquid continues to crystalize, further enriching the residual liquid to the REE concentrations which are estimated by the inversions of individual phases.

30% ur-KREEP (Snyder et al., 1992) and 70% 15426 green glass beads (Borg et al., 2019). In this exercise, a zircon REE concentration from Whitehouse and Nemchin (2009) is used as a stand-in for possible HREE-rich phases in Mg-suite samples (baddeleyite, merrillite, and zircons). The result of this exercise is that the HREE depletion in the parental liquid can be explained by 3-4% zircon fractionation, implying that a minor amount of HREE phase needs to be fractionated to explain the REE composition of the parental liquid. (see figure 12). Although not a major phase within Mg-suite samples, zircons and baddeleyite have been identified within Mg-suite troctolites, norites, and breccias. The ages of these zircons within Apollo and meteoritic Mg-suite samples are 4.332 ± 18 Ga and 4.354 ± 76 Ga, respectively (Zhang et al., 2021; Zhang et al., 2023). These ages coincide with the proposed pulse of Mg-suite magmatism at 4.4~4.3 Ga and a peak in zircon formation on the Moon at 4.33 Ga (Barboni et al., 2024), alluding to the possibility that the zircon formation and Mg-suite may be petrogenetically related such as a process proposed in this study. However, understanding the effects that ur-KREEP assimilation has on the major element chemistry and the phase equilibria (phase compositions and proportions) within the Mg-suite is beyond the scope of the present study and would require dedicated investigation in the future.

CONCLUSIONS

We measured major elements and thirty-three trace elements in plagioclase grain separates from troctolite 76535. The REE contents of these grains are consistent with known Mg-suite trends, namely, highly calcic plagioclase with enrichments in LREEs. The results of the microanalyses

also provide evidence for the preservation of the magmatic concentrations within these grains. The samples exhibit high inter and intra-grain homogeneity and are likely sourced from the cores of cumulus plagioclase grains, given the lack of the predicted diffusion profiles. Using these measurements, we estimated the unfractionated Mg-suite parental liquid using a python-based forward model and a RhyoliteMELTS-defined LLD.

The estimated parental liquid contains enrichments of LREEs ~100 times chondrite, which decreases towards the HREEs being enriched only to ~ 10 times chondrite. Inversions of REE data from 76535 and other Mg-suite samples predict more enriched liquids, which may represent the continued fractionation of the Mg-suite parental liquid.

This study constrains the formation and crystallization of 76535 from the Mg-suite parental melt and establishes limits for the ur-KREEP contribution to the primary Mg-suite melt. Mixing and fractionation exercises indicate that the estimated Mg-suite parental liquid could be explained by the assimilation of 30-40% ur-KREEP material if the primary liquid is highly REE-depleted. Additionally, the fractionation of 4% zircon by weight may be necessary to account for the observed HREE depletion in the estimated parental melt.

This study demonstrates that the geochemical characterization of only a few mineral grains can provide key information about the petrogenesis of a lunar sample. We therefore present an approach of maximizing scientific output from returned planetary samples in the future, including the Artemis missions.

ACKNOWLEDGEMENTS

We are grateful to the AARB for loaning these samples to us and Ryan Ziegler (JSC, Houston) for assisting us in the sample request process. We acknowledge the NASA Cosmochemistry, Emerging Worlds, and Planetary Major Equipment Programs and the NSF Major Research Instrumentation Program for funding of the instrumentation in the Kuiper Materials Imaging and Characterization Facility at the University of Arizona. SIMS analysis at Arizona State University was supported by NSF EAR 1819550. LA-ICP-MS analyses were performed with support from the Lowell IMR Mineral Characterization Facility. We would like to thank Katherine Kelley (University of Rhode Island) and Esteban Gazel (Cornell University) for their advice on the laser ablation analyses, and Chip Shearer (University of New Mexico), Chenguang Sun (Brown University), and Arkadeep Roy (University of Arizona) for helpful insights into this work. IS acknowledges graduate funding from the University of Arizona Galileo Circle; The Community Foundation for Southern AZ; and the Spencer R Titley Grad Fellowship and AM acknowledges NASA grant 80NSSC24K0543 and start-up funds from the Eminent Scholars Program managed by the Office of the Provost and the University of Arizona Foundation. We also thank Karla Tellez for assisting with organizing the supplemental materials.

Appendix A. Forward model parameters

The basis for the forward model is a fractional crystallization sequence calculated in AlphaMELTS. The input for this fractional crystallization sequence is included in the supplementary materials and outlines the content of the major oxides, the fO_2 buffer, the initial and final temperatures and pressures, and the type of fractionation. The file containing the major element oxide mass fractions, which was input into RhyoliteMELTS, and the various output files are available in the supplemental materials. These oxide concentrations were taken from Prissel et al. (2016), who adapted the Mg-suite parental melt composition from Longhi et al. (2010),

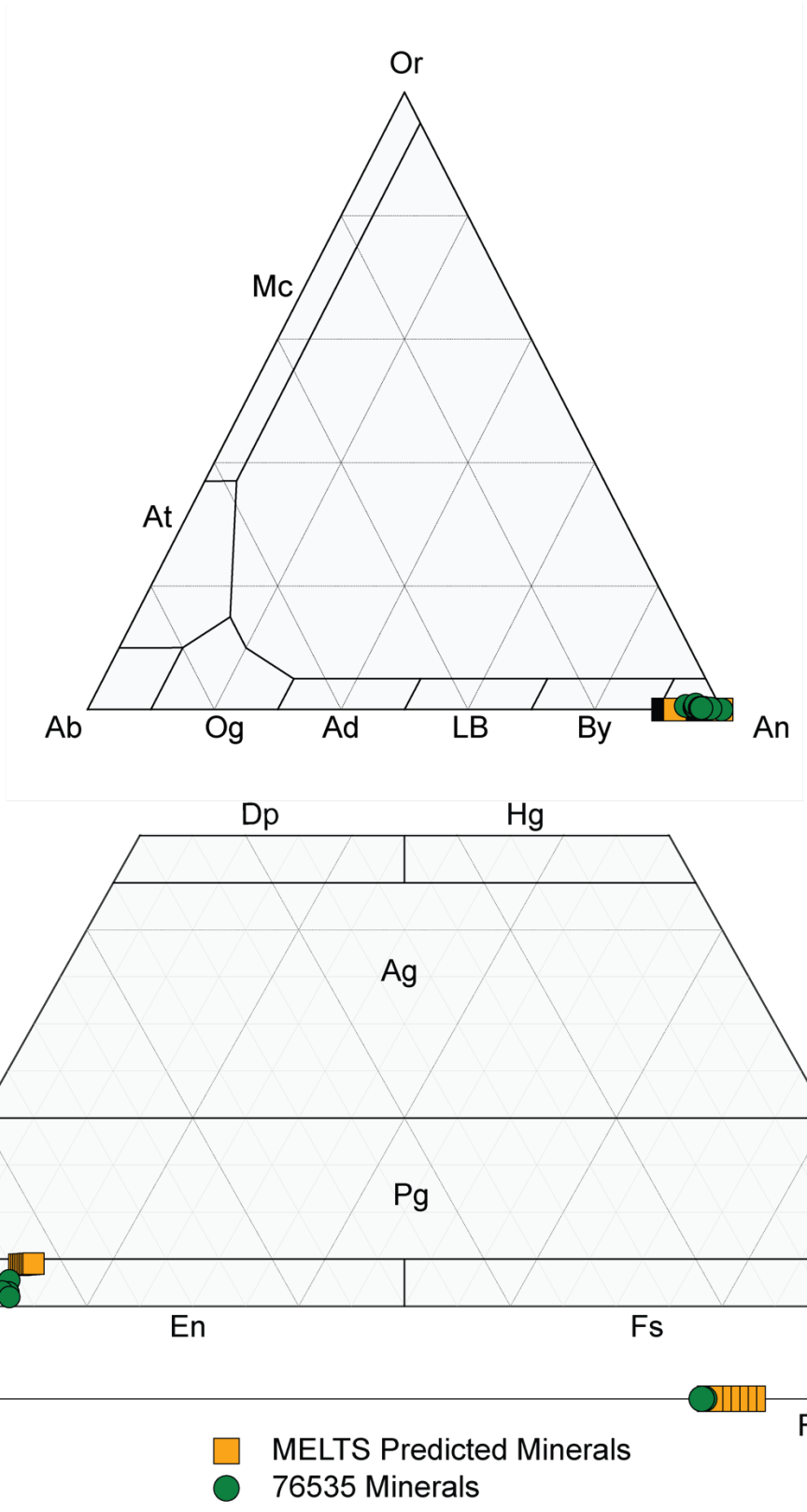
Or
Mc
At
Ab
Og
Ad
LB
By
An
Dp
Hg
Ag
Pg
En
Fs
Fa
Fo
MELTS Predicted Minerals
76535 Minerals

520

Figure 14. phase diagrams comparing major compositions of 76535 minerals to mineral compositions modeled by RhyoliteMELTS (Gualda et al., 2012; Ghiorso et al., 1995; Asimow and Ghiorso, 1998). The modeled minerals show a limited compositional range and therefore are a close match to 76535 minerals throughout the LLD.

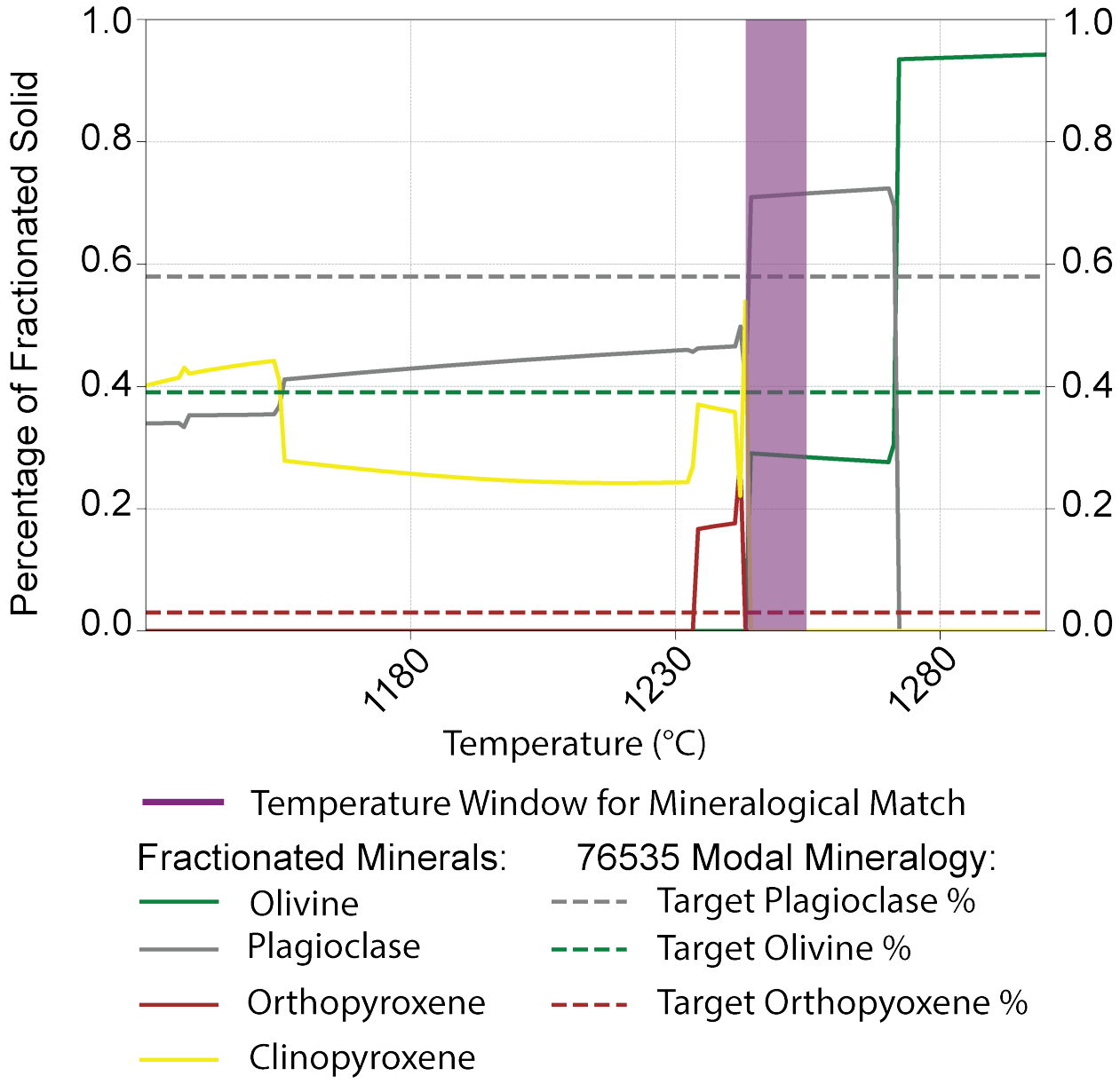

Figure 15. Mineralogy of fractionated minerals at each temperature of RhyoliteMELTS (Gualda et al., 2012; Ghiorso et al., 1995; Asimow and Ghiorso, 1998) fractional crystallization sequence. The Purple bar represents the range of temperatures in which the fractionated minerals most closely match the minerals of 76535 which was used in the forward model.

521 which represents a likely composition of the Mg-suite parental liquid. Due to the limitations of

the RhyoliteMELTS 1.0.2 software, Mn and K were excluded from the parental liquid. The fO_2 buffer was set at IW consistent with the lunar upper mantle (Herd, 2008; Wadhwa, 2008). The initial temperature was set at 1500 °C, and the final temperature was set at 900 °C. The temperature was set to 0.26 GPa, corresponding to multiple geobarometry calculations for 76535 (Gooley et al., 1974; McCallum and O'Brien, 1996; Schwartz and McCallum, 1999, 2001; White et al., 2020). The outputs from the crystallization sequence are available in the supplementary material., Figure 13 shows the mineralogy of the major phases (Plagioclase, Olivine, and Orthopyroxene) as predicted by RhyoliteMELTS in comparison to the composition of 76535 minerals.

Appendix B. Supplementary material

Supplementary material related to this article can be found online at (Link)

Data Sharing and Data Accessibility

The data (raw EPMA, SIMS, and LA-ICP-MS data, Homogeneity calculations, and RhyoliteMELTS inputs and output files) that support the findings of this study are available upon request. The Python scripts used in the calculation of the unfractionated parental liquid and the inversions of plagioclase data are available from the corresponding author upon reasonable request.

REFERENCES

Anderson, G. M. (1976). Error propagation by the Monte Carlo method in geochemical calculations. Geochimica et Cosmochimica Acta, 40(12), 1533-1538.

Asimow, P. D., & Ghiorso, M. S. (1998). Algorithmic modifications extending MELTS to calculate subsolidus phase relations. *American Mineralogist*, *83*(9-10), 1127-1132.

Barboni, M., Szymanowski, D., Schoene, B., Dauphas, N., Zhang, Z. J., Chen, X., & McKeegan, K. D. (2024). High-precision U-Pb zircon dating identifies a major magmatic event on the Moon at 4.338 Ga. *Science Advances*, *10*(30), eadn9871.

Blundy, J., & Wood, B. (2003). Partitioning of trace elements between crystals and melts. Earth and Planetary Science Letters, 210(3-4), 383-397.

Bogard, D. D., Nyquist, L. E., Bansal, B. M., Wiesmann, H., & Shih, C. Y. (1975). 76535: An old lunar rock. *Earth and Planetary Science Letters*, *26*(1), 69-80.

Borg, L. E., Gaffney, A. M., & Shearer, C. K. (2015). A review of lunar chronology revealing a preponderance of 4.34–4.37 Ga ages. *Meteoritics & Planetary Science*, *50*(4), 715-732.

Borg, L. E., Connelly, J. N., Cassata, W. S., Gaffney, A. M., & Bizzarro, M. (2017). Chronologic implications for slow cooling of troctolite 76535 and temporal relationships between the Mg-suite and the ferroan anorthosite suite. Geochimica et Cosmochimica Acta, 201, 377-391.

Borg, L. E., Gaffney, A. M., Kruijer, T. S., Marks, N. A., Sio, C. K., & Wimpenny, J. (2019). Isotopic evidence for a young lunar magma ocean. Earth and Planetary Science Letters, 523, 115706.

Borg, L. E., Cassata, W. S., Wimpenny, J., Gaffney, A. M., & Shearer, C. K. (2020). The formation and evolution of the Moon's crust inferred from the Sm-Nd isotopic systematics of highlands rocks. *Geochimica et Cosmochimica Acta*, *290*, 312-332.

Cahill, J. T. S., Lucey, P. G., & Wieczorek, M. A. (2009). Compositional variations of the lunar crust: Results from radiative transfer modeling of central peak spectra. Journal of Geophysical Research: Planets, 114(E9).

Cao, H., Ling, Z., Chen, J., Fu, X., & Zou, Y. (2021). Petrography, mineralogy, and geochemistry of a new lunar magnesian feldspathic meteorite Northwest Africa 11460. Meteoritics & Planetary Science, 56(10), 1857-1889.

Cherniak, D. J. (2003). REE diffusion in feldspar. *Chemical Geology*, *193*(1-2), 25-41.

Dymek, R. F., Albee, A. L., & Chodos, A. A. (1975). Comparative petrology of lunar cumulate rocks of possible primary origin-Dunite 72415, troctolite 76535, norite 78235, and anorthosite 62237. In In: Lunar Science Conference, 6th, Houston, Tex., March 17-21, 1975, Proceedings. Volume 1. (A78-46603 21-91) New York, Pergamon Press, Inc., 1975, p. 301-341. (Vol. 6, pp. 301-341).

Edmunson, J., Borg, L. E., Nyquist, L. E., & Asmerom, Y. (2009). A combined Sm–Nd, Rb–Sr, and U–Pb isotopic study of Mg-suite norite 78238: further evidence for early differentiation of the Moon. *Geochimica et Cosmochimica Acta*, *73*(2), 514-527.

Elardo, S. M., McCubbin, F. M., & Shearer Jr, C. K. (2012). Chromite symplectites in Mg-suite troctolite 76535 as evidence for infiltration metasomatism of a lunar layered intrusion. Geochimica et Cosmochimica Acta, 87, 154-177.

Elardo, S. M., Laneuville, M., McCubbin, F. M., & Shearer, C. K. (2020). Early crust building enhanced on the Moon's nearside by mantle melting-point depression. *Nature Geoscience*, *13*(5), 339-343.

Tanton, L. T. E., Van Orman, J. A., Hager, B. H., & Grove, T. L. (2002). Re-examination of the lunar magma ocean cumulate overturn hypothesis: melting or mixing is required. Earth and Planetary Science Letters, 196(3-4), 239-249.

Gaffney, A. M., & Borg, L. E. (2014). A young solidification age for the lunar magma ocean. Geochimica et Cosmochimica Acta, 140, 227-240.

610 Ghiorso, M. S., & Sack, R. O. (1995). Chemical mass transfer in magmatic processes IV. A
611 revised and internally consistent thermodynamic model for the interpolation and extrapolation of
612 liquid-solid equilibria in magmatic systems at elevated temperatures and pressures. Contributions
613 to Mineralogy and Petrology, 119, 197-212.
614
615 Gooley, R., Brett, R., Warner, J., & Smyth, J. R. (1974). A lunar rock of deep crustal origin:
616 Sample 76535. Geochimica et Cosmochimica Acta, 38(9), 1329-1339.
617
618 Gross, J., Hilton, A., Prissel, T. C., Setera, J. B., Korotev, R. L., & Calzada-Diaz, A. (2020).
619 Geochemistry and petrogenesis of Northwest Africa 10401: A new type of the Mg-suite rocks.
620 *Journal of Geophysical Research: Planets*, *125*(5), e2019JE006225.
621
622 Harries, D. (2014). Homogeneity testing of microanalytical reference materials by electron probe
623 microanalysis (EPMA). *Geochemistry*, *74*(3), 375-384.
624
625 Haskin, L. A., Shih, C. Y., Bansal, B. M., Rhodes, J. M., Wiesmann, H., & Nyquist, L. E.
626 (1974). Chemical evidence for the origin of 76535 as a cumulate. In In: Lunar Science
627 Conference, 5th, Houston, Tex., March 18-22, 1974, Proceedings. Volume 2. (A75-39540 19-91)
628 New York, Pergamon Press, Inc., 1974, p. 1213-1225. (Vol. 5, pp. 1213-1225).
629
630 He, Q., Cao, Z., Qian, Y., Hui, H., Baziotis, I., Xiao, L., ... & Li, Y. (2024). Petrogenesis of
631 magnesian troctolitic granulite clasts from Chang'e-5 drilling sample: Implications for the origin
632 of ejecta material from lunar highlands. *Icarus*, *408*, 115853.
633
634 Herd, C. D. (2008). Basalts as probes of planetary interior redox state. Reviews in Mineralogy
635 and Geochemistry, 68(1), 527-553.
636
637 Hess, P.C., Rutherford, M.J., and Campbell, H.W. (1978) Ilmenite crystallization in
638 non-mare basalt: Genesis of KREEP and high-Ti mare basalts. Proceedings 9th
639 Lunar Science Conference, 705–724.
640
641 Hess, P.C. (1989) Origin of Igneous Rocks, 336 p. Harvard University Press, Cambridge,
642 Massachusetts.
643
644 Hess, P.C. (1994) The petrogenesis of lunar troctolites. Journal of Geophysical Research,
645 99(E9), 19083–19093.
646
647 Hinton, R. W. (1990). Ion microprobe trace-element analysis of silicates: Measurement of multi-
648 element glasses. *Chemical Geology*, *83*(1-2), 11-25.
649
650 Hulsey, C. R., & O'Sullivan, K. M. (2024). Petrographic and geochemical analysis of lunar
651 meteorite NWA 11788: Parallels with Luna 20 and the Apollo magnesian granulites. *Meteoritics*
652 *& Planetary Science*, *59*(10), 2744-2768.
653

654 Irving, A. J. (1978). A review of experimental studies of crystal/liquid trace element partitioning.
655 Geochimica et Cosmochimica Acta, 42(6), 743-770.
656
657 James, O.B., and Flohr, M.K. (1983) Subdivision of the Mg-suite noritic rocks into
658 Mg-gabbronorites and Mg-norites. Journal of Geophysical Research, 88, Suppl.
659 A603–A614.
660
661 Jolliff, B. L., Gillis, J. J., Haskin, L. A., Korotev, R. L., & Wieczorek, M. A. (2000). Major lunar
662 crustal terranes: Surface expressions and crust-mantle origins. *Journal of Geophysical Research:*
663 *Planets*, *105*(E2), 4197-4216.
664
665 Klima, R. L., Pieters, C. M., Boardman, J. W., Green, R. O., Head III, J. W., Isaacson, P. J., ... &
666 Tompkins, S. (2011). New insights into lunar petrology: Distribution and composition of
667 prominent low-Ca pyroxene exposures as observed by the Moon Mineralogy Mapper (M3).
668 *Journal of Geophysical Research: Planets*, *116*(E6).
669
670 Kuehn, S. C. (2016). Routine EPMA of silicate glasses using a 5 micron beam: taking advantage
671 of TDI, combined EDS+ WDS, MAN, and a multi-standard blank correction. In Program guide
672 with abstracts, Microanalysis Society Topical Conference-Electron-Probe Microanalysis (EPMA
673 2016). University of Wisconsin-Madison, WI, May (pp. 16-19).
674
675 Laneuville, M. (2013). *Thermal evolution of the Moon* (Doctoral dissertation, Institut de
676 Physique du Globe de Paris).
677
678 Lawrence, D. J., Feldman, W. C., Barraclough, B. L., Binder, A. B., Elphic, R. C., Maurice, S.,
679 ... & Prettyman, T. H. (2000). Thorium abundances on the lunar surface. *Journal of Geophysical*
680 *Research: Planets*, *105*(E8), 20307-20331.
681
682 Longhi, J., and Boudreau, A.E. (1979) Complex igneous processes and the formation
683 of the primitive lunar crustal rocks. Proceedings 10th Lunar Planetary Science
684 Conference 2085–2105.
685
686 Longhi, J., Durand, S. R., & Walker, D. (2010). The pattern of Ni and Co abundances in lunar
687 olivines. Geochimica et Cosmochimica Acta, 74(2), 784-798.
688
689 Martinot, M., Flahaut, J., Besse, S., Quantin-Nataf, C., & Van Westrenen, W. (2020).
690 Mineralogical survey of the anorthositic Feldspathic Highlands Terrane crust using Moon
691 Mineralogy Mapper data. *Icarus*, *345*, 113747.
692
693 Maurice, M., Tosi, N., Schwinger, S., Breuer, D., & Kleine, T. (2020). A long-lived magma
694 ocean on a young Moon. Science advances, 6(28), eaba8949.
695
696 McCallum, I.S. (1983) Formation of Mg-rich pristine rocks by crustal metasomatism.
697 Lunar and Planetary Science XIV, 473–474.
698

McCallum, I.S., and O'Brien, H.E. (1996) Stratigraphy of the lunar highland crust: Depths of burial of lunar samples from cooling-rate studies. American Mineralogist, 81, 1166–1175.

McCallum, I. S., & Schwartz, J. M. (2001). Lunar Mg suite: Thermobarometry and petrogenesis of parental magmas. Journal of Geophysical Research: Planets, 106(E11), 27969-27983.

McDonough, W. F., & Sun, S. S. (1995). The composition of the Earth. Chemical geology, 120(3-4), 223-253.

Nelson, W. S., Hammer, J. E., Shea, T., Hellebrand, E., & Jeffrey Taylor, G. (2021). Chemical heterogeneities reveal early rapid cooling of Apollo Troctolite 76535. Nature Communications, 12(1), 7054.

Nord Jr, G. L., Christie, J. M., Lally, J. S., & Heuer, A. H. (1977). The thermal and deformational history of Apollo 15418, a partly shock-melted lunar breccia. *The moon*, *17*(3), 217-231.

McKay, D. S., & Williams, R. J. (1979). A geologic assessment of potential lunar ores. Space resources and space settlements, 1, 243-255.

Paton, C., Hellstrom, J., Paul, B., Woodhead, J., & Hergt, J. (2011). Iolite: Freeware for the visualisation and processing of mass spectrometric data. *Journal of Analytical Atomic Spectrometry*, *26*(12), 2508-2518.

Paul, B., Petrus, J., Savard, D., Woodhead, J., Hergt, J., Greig, A., ... & Rayner, P. (2023). Time resolved trace element calibration strategies for LA-ICP-MS. *Journal of Analytical Atomic Spectrometry*, *38*(10), 1995-2006.

Papanastassiou, D. A., & Wasserburg, G. J. (1976). Rb-Sr age of troctolite 76535. In *In: Lunar Science Conference, 7th, Houston, Tex., March 15-19, 1976, Proceedings. Volume 2.(A77-34651 15-91) New York, Pergamon Press, Inc., 1976, p. 2035-2054.* (Vol. 7, pp. 2035-2054).

Papike, J. J., Fowler, G. W., & Shearer, C. K. (1994). Orthopyroxene as a recorder of lunar crust evolution: An ion microprobe investigation of Mg-suite norites. *American Mineralogist*, *79*(7-8), 796-800.

Papike, J. J., Fowler, G. W., Shearer, C. K., & Layne, G. D. (1996). Ion microprobe investigation of plagioclase and orthopyroxene from lunar Mg-suite norites: Implications for calculating parental melt REE concentrations and for assessing postcrystallization REE redistribution. Geochimica et Cosmochimica Acta, 60(20), 3967-3978.

Papike, J. J., Ryder, G., & Shearer, C. K. (1998). Lunar samples. Planetary materials, 36(5), 1-234.

Prissel, T. C., Parman, S. W., Jackson, C. R. M., Rutherford, M. J., Hess, P. C., Head, J. W., ... & Pieters, C. M. (2014). Pink Moon: The petrogenesis of pink spinel anorthosites and implications concerning Mg-suite magmatism. *Earth and Planetary Science Letters*, *403*, 144-156.

Prissel, T. C., Parman, S. W., & Head, J. W. (2016). Formation of the lunar highlands Mg-suite as told by spinel. American Mineralogist, 101(7), 1624-1635.

Prissel, T. C., Zhang, N., Jackson, C. R., & Li, H. (2023). Rapid transition from primary to secondary crust building on the Moon explained by mantle overturn. Nature Communications, 14(1), 5002.

Roberts, S. E., McCanta, M. C., Jean, M. M., & Taylor, L. A. (2019). New lunar meteorite NWA 10986: A mingled impact melt breccia from the highlands—A complete cross section of the lunar crust. *Meteoritics & Planetary Science*, *54*(12), 3018-3035.

Schwartz, J. M., & McCallum, I. S. (1999). Inferred Depths of Formation of Spinel Cataclasites and Troctolitic Granulite, 76535 Using New Thermodynamic Data for Cr-Spinel. In Lunar and Planetary Science Conference (p. 1308).

Shearer, C.K., and Floss, C. (2000) Evolution of the Moon's mantle and crust as reflected in trace element microbeam studies of lunar magmatism. In R. Canup and K. Righter, Eds., Origin of the Earth and Moon, p. 339–359. University of Arizona Press, Tuscon.

Shearer, C.K., and Papike, J.J. (1999) Magmatic evolution of the Moon. American Mineralogist, 84, 1469–1494.

Shearer, C.K., and Papike, J.J. (2005) Early crustal building processes on the Moon: models for the petrogenesis of the Mg-suite. Geochimica et Cosmochimica Acta, 69(13), 3445–3461.

Shearer, C. K., Hess, P. C., Wieczorek, M. A., Pritchard, M. E., Parmentier, E. M., Borg, L. E., ... & Wiechert, U. (2006). Thermal and magmatic evolution of the Moon. Reviews in Mineralogy and Geochemistry, 60(1), 365-518.

Shearer, C. K., Elardo, S. M., Petro, N. E., Borg, L. E., & McCubbin, F. M. (2015). Origin of the lunar highlands Mg-suite: An integrated petrology, geochemistry, chronology, and remote sensing perspective. American Mineralogist, 100(1), 294-325.

Sheikh, D., Ruzicka, A. M., & Hutson, M. L. (2024). "Ground Truth" Occurrence of Pink Spinel Anorthosite (PSA) as Clasts in Lunar Meteorite Northwest Africa (NWA) 15500: Chemical Evidence for a Genetic Relationship with Lunar Highlands Mg-suite and Formation by Magma–Wallrock Interactions. Meteoritics & Planetary Science.

787 Shervais, J. W., & McGee, J. J. (1998). Ion and electron microprobe study of troctolites, norite,
788 and anorthosites from Apollo 14: Evidence for urKREEP assimilation during petrogenesis of
789 Apollo 14 Mg-suite rocks. Geochimica et Cosmochimica Acta, 62(17), 3009-3023.
790
791 Snape, J. F., Nemchin, A. A., Bellucci, J. J., Whitehouse, M. J., Tartèse, R., Barnes, J. J., ... &
792 Joy, K. H. (2016). Lunar basalt chronology, mantle differentiation and implications for
793 determining the age of the Moon. Earth and Planetary Science Letters, 451, 149-158.
794
795 Snyder, G. A., Taylor, L. A., & Neal, C. R. (1992). A chemical model for generating the sources
796 of mare basalts: Combined equilibrium and fractional crystallization of the lunar magmasphere.
797 Geochimica et Cosmochimica Acta, 56(10), 3809-3823.
798
799 Snyder, G. A., Neal, C. R., Taylor, L. A., & Halliday, A. N. (1995). Processes involved in the
800 formation of magnesian-suite plutonic rocks from the highlands of the Earth's Moon. *Journal of*
801 *Geophysical Research: Planets*, *100*(E5), 9365-9388.
802
803 Snyder, G. A., Taylor, L. A., Patchen, A., Nazarov, M. A., & Semenova, T. S. (1999, March).
804 Mineralogy and petrology of a primitive spinel troctolite and gabbros from Luna 20, eastern
805 highlands of the Moon. In Lunar and planetary science conference (p. 1491).
806
807 Sun, C., & Liang, Y. (2014). An assessment of subsolidus re-equilibration on REE distribution
808 among mantle minerals olivine, orthopyroxene, clinopyroxene, and garnet in peridotites.
809 Chemical Geology, 372, 80-91.
810
811 Sun, C., Graff, M., & Liang, Y. (2017). Trace element partitioning between plagioclase and
812 silicate melt The importance of temperature and plagioclase composition, with implications for
813 terrestrial and lunar magmatism. Geochimica et Cosmochimica Acta, 206, 273-295.
814
815 Tatsumoto, M., Premo, W. R., & Unruh, D. M. (1987). Origin of lead from green glass of Apollo
816 15426: A search for primitive lunar lead. Journal of Geophysical Research: Solid Earth, 92(B4),
817 E361-E371.
818
819 Taylor, G. J. (2009). Ancient lunar crust: Origin, composition, and implications. Elements, 5(1),
820 17-22.
821
822 Taylor, S.R., Norman, M.D., and Esat, T.M. (1993) The Mg-suite and the highland crust:
823 An unsolved enigma. Proceedings 24th Lunar and Planetary Science Conference,
824 1413–1414.
825
826 Treiman, A. H. (1996). The perils of partition: Difficulties in retrieving magma compositions
827 from chemically equilibrated basaltic meteorites. Geochimica et Cosmochimica Acta, 60(1),
828 147-155.
829

Treiman, A. H., Maloy, A. K., Shearer Jr, C. K., & Gross, J. (2010). Magnesian anorthositic granulites in lunar meteorites Allan Hills A81005 and Dhofar 309: Geochemistry and global significance. *Meteoritics & Planetary Science*, *45*(2), 163-180.

Treiman, A. H., & Gross, J. (2015). A rock fragment related to the magnesian suite in lunar meteorite Allan Hills (ALHA) 81005. American Mineralogist, 100(2-3), 414-426.

Wadhwa, M. (2008). Redox conditions on small bodies, the Moon and Mars. Reviews in Mineralogy and Geochemistry, 68(1), 493-510.

Warner, J. L., Simonds, C. H., & Phinney, W. C. (1976). Apollo 17, Station 6 boulder sample 76255: Absolute petrology of breccia matrix and igneous clasts. Pergamon Press.

Warren, P.H., and Wasson, J.T. (1977) Pristine nonmare rocks and the nature of the lunar crust. Proceedings 8th Lunar Science Conference, 2215–2235.

Warren, P. H. (1986). The bulk-Moon MgO/FeO ratio: A highlands perspective. In *Origin of the Moon* (p. 279).

Warren, P. H. (1989). KREEP: major-element diversity, trace-element uniformity (almost). In Moon in transition: Apollo 14, KREEP, and evolved lunar rocks (pp. 149-153).

Warren, P. H. (1993). A concise compilation of petrologic information on possibly pristine nonmare Moon rocks. American Mineralogist, 78(3-4), 360-376.

White, L. F., Černok, A., Darling, J. R., Whitehouse, M. J., Joy, K. H., Cayron, C., ... & Anand, M. (2020). Evidence of extensive lunar crust formation in impact melt sheets 4,330 Myr ago. Nature Astronomy, 4(10), 974-978.

Wood, J.A. (1975) Lunar petrogenesis in a well-stirred magma ocean. Proceedings 6th Lunar Science Conference, 1087–1102.

Whitehouse, M. J., & Nemchin, A. A. (2009). High precision, high accuracy measurement of oxygen isotopes in a large lunar zircon by SIMS. Chemical Geology, 261(1-2), 32-42.

Wopenka, B., Jolliff, B., Zinner, E. & Kremser, D. (1996). Trace element zoning and incipient metamictization in a lunar zircon: Application of three microprobe techniques. *American Mineralogist*, *81*(7-8), 902-912.

Yamaguchi, A., Karouji, Y., Takeda, H., Nyquist, L., Bogard, D., Ebihara, M., ... & McKay, G. (2010). The variety of lithologies in the Yamato-86032 lunar meteorite: Implications for formation processes of the lunar crust. Geochimica et Cosmochimica Acta, 74(15), 4507-4530.

873 Zhang, B., Lin, Y., Hao, J., Schrader, D. L., Wadhwa, M., Korotev, R. L., ... & Bouvier, A.
874 (2023). SIMS U-Pb dating of micro-zircons in the lunar meteorites Dhofar 1528 and Dhofar
875 1627. *Meteoritics & Planetary Science*, *58*(10), 1540-1551.
876
877 Zhang, B., Lin, Y., Moser, D. E., Warren, P. H., Hao, J., Barker, I. R., ... & Bouvier, A. (2021).
878 Timing of lunar Mg-suite magmatism constrained by SIMS U-Pb dating of Apollo norite 78238.
879 *Earth and Planetary Science Letters*, *569*, 117046.